AD-A044 539 ARMY ARMAMENT RESEARCH AND DEVELOPMENT COMMAND DOVER--ETC F/G 19/4
PANOL SIX DEGREES-OF-FREEDOM SYSTEM ANALYSIS AND USAGE.(U)
SEP 77 E M FRIEDMAN

UNCLASSIFIED ARLCD-TR-77025

1 OF 2
AD
A044 539

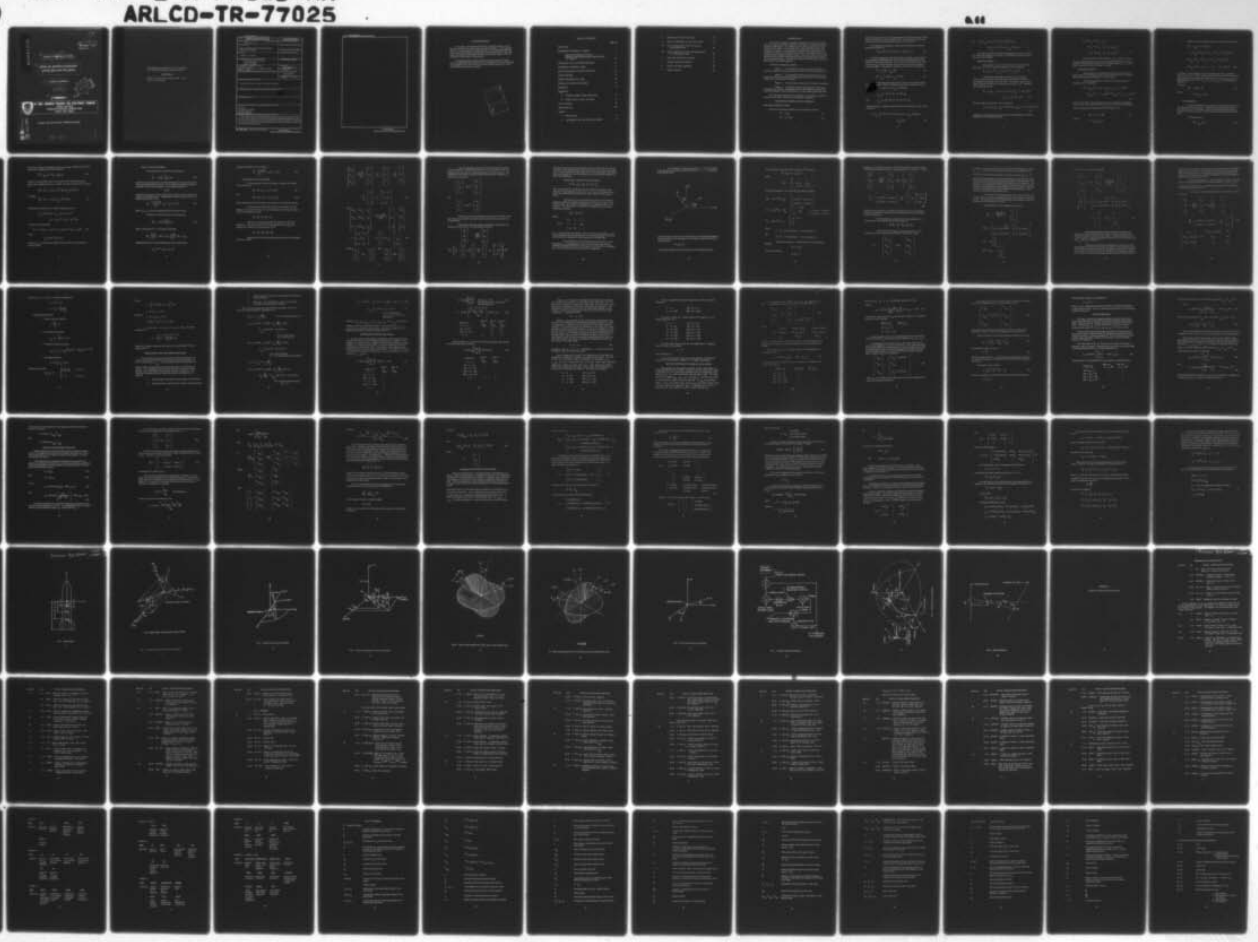

12
B.S

(9) (14) TECHNICAL REPORT ARLCD-TR-77025

(6) PANOL SIX DEGREES-OF-FREEDOM SYSTEM ANALYSIS AND USAGE.

(10) EUGENE M. FRIEDMAN

(12) 148 p.

(11) SEPT[redacted]977

US ARMY ARMAMENT RESEARCH AND DEVELOPMENT COMMAND
LARGE CALIBER
WEAPON SYSTEMS LABORATORY
DOVER, NEW JERSEY

APPROVED FOR PUBLIC RELEASE; DISTRIBUTION UNLIMITED.

410 163

The findings in this report are not to be construed as an official Department of the Army position.

DISPOSITION

Destroy this report when no longer needed. Do not return to the originator.

UNCLASSIFIED
SECURITY CLASSIFICATION OF THIS PAGE (When Data Entered)

REPORT DOCUMENTATION PAGE		READ INSTRUCTIONS BEFORE COMPLETING FORM
1. REPORT NUMBER ARLCD-TR-77025	2. GOVT ACCESSION NO.	3. RECIPIENT'S CATALOG NUMBER
4. TITLE (and Subtitle) PANOL SIX DEGREES-OF-FREEDOM SYSTEM ANALYSIS AND USAGE		5. TYPE OF REPORT & PERIOD COVERED 6. PERFORMING ORG. REPORT NUMBER
7. AUTHOR(s) Eugene M. Friedman		8. CONTRACT OR GRANT NUMBER(s)
9. PERFORMING ORGANIZATION NAME AND ADDRESS Feltman Research Laboratory Picatinny Arsenal Dover, NJ 07801		10. PROGRAM ELEMENT, PROJECT, TASK AREA & WORK UNIT NUMBERS
11. CONTROLLING OFFICE NAME AND ADDRESS ARRADCOM, LCWSL Applied Sciences Division (DRDAR-LCA-FB) Dover, NJ 07801		12. REPORT DATE SEPTEMBER 1977 13. NUMBER OF PAGES 116
14. MONITORING AGENCY NAME & ADDRESS(if different from Controlling Office)		15. SECURITY CLASS. (of this report) UNCLASSIFIED 15a. DECLASSIFICATION/DOWNGRADING SCHEDULE

16. DISTRIBUTION STATEMENT (of this Report)

Approved for public release; distribution unlimited.

17. DISTRIBUTION STATEMENT (of the abstract entered in Block 20, if different from Report)

18. SUPPLEMENTARY NOTES

19. KEY WORDS (Continue on reverse side if necessary and identify by block number)

Trajectory
Six degrees of freedom
Precision munitions
Controlled missile

20. ABSTRACT (Continue on reverse side if necessary and identify by block number)

A description is given of the development and execution of a system of computer programs which describe the motion of a projectile in six degrees of freedom. Several versions of PANOL exist which can simulate the flight of a projectile: with body-fixed aerodynamic asymmetry, with mass asymmetry, with a yaw sonde on board, or with guidance and steering jets.

DD FORM 1 JAN 73 1473 EDITION OF 1 NOV 65 IS OBSOLETE

UNCLASSIFIED
SECURITY CLASSIFICATION OF THIS PAGE (When Data Entered)

ACKNOWLEDGMENTS

This report, which describes a family of computer codes, is substantially based on the earlier reports of DeGrafft (Ref 1, 2) and Gerhard (Ref 3), as is the program, though both have been substantially modified. In the interests of clarity and to document new additions to the codes, this report will duplicate substantial sections of the earlier reports, with the permission of the authors' organizations.

The mathematical gyroscope model and its description are taken from an unpublished description by Dr. Gene Hopkins of Texas Instruments as developed for the TLGP (Tube Launched Guided Projectile) for which we would like to express our thanks.

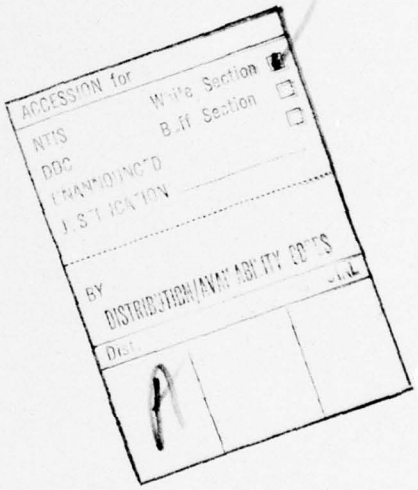

TABLE OF CONTENTS

INTRODUCTION

The family of computer programs described in this report all calculate a six degree of freedom simulation of the flight of a rigid body through the earth's atmosphere. The elements of the transformation matrix from inertial axis to body axis are produced by direct integration rather than through Euler angles. Aerodynamic force and moment coefficients are introduced as tables as a function of Mach number, total angle of attack, and roll position of the plane of angle of attack. They are so written as to make the use of body-fixed axes possible even when the integration proceeds in non-rolling coordinates. The vehicle is allowed an initial coast, a powered phase, and a final coasting phase.

The family of programs includes:

PANOL 2 - for symmetric missiles and projectiles where products of inertia vanish and the center of mass is on the longitudinal axis.

PANOL 3 - for unsymmetric missiles and projectiles where products of inertia may appear and the center of mass may lie off the longitudinal axis, but the mass is constant.

PANOL 4 - for yaw sonde simulations of symmetric projectiles.

PANOL 5 - for guided missiles and projectiles with a target consisting of an upright, rectangular plane subdivided into rectangles of varying brightness; with thrust control; on a non-rotating spherical earth.

The computer program input instructions are included as Appendix A. Output formats, titles, and units are contained in Appendix B.

MATHEMATICAL FORMULATION OF PROBLEM

Rigid Body Equations of Motion

The force and moment equations can be written in the form

$$\vec{F} = \int \vec{a}\, dm \tag{1}$$

$$\vec{M} = \int \vec{r} \times \vec{a}\, dm \tag{2}$$

These integrals extend over all mass particles within the geometric boundary of the vehicle at a given instant of time. This boundary lies on the vehicle surface and includes the rocket nozzle exit surface.

The absolute acceleration of a mass particle within the vehicle's geometric boundary is

$$\vec{a} = \vec{a}_o + \dot{\vec{\omega}} \times \vec{r} + \vec{\omega} \times (\vec{\omega} \times \vec{r}) + 2\vec{\omega} \times \vec{V}_r + \vec{a}_r \tag{3}$$

The mass contained within the geometric boundary of the vehicle at any instant is composed of the mass of the vehicle structure and the mass of the unburned propellant, the sum being designated as m_s, plus the mass (m_g) of the propellant gases which have not yet crossed the nozzle exit plane. Accordingly, Equations 1 and 2 can be rewritten as

$$\vec{F} = \int_{m_s} \vec{a}\, dm + \int_{m_g} \vec{a}\, dm \tag{4}$$

$$\vec{M} = \int_{m_s} \vec{r} \times \vec{a}\, dm + \int_{m_g} \vec{r} \times \vec{a}\, dm \tag{5}$$

For the time being the computational axes will be rigidly fixed to the vehicle so that in the first integral appearing in Equations 4 and 5, $\vec{V}$ = o. Also, since $m_s >> m_g$, the integrals

$$\int_{m_g} [\vec{a}_o + \dot{\vec{\omega}} \times \vec{r} + \vec{\omega} \times (\vec{\omega} \times \vec{r})]\, dm$$

and $$\int_{m_g} \vec{r} \times [\vec{a}_o + \dot{\vec{\omega}} \times \vec{r} + \vec{\omega} \times (\vec{\omega} \times \vec{r})]\, dm$$

will be neglected. Subject to these restrictions, Equations 4 and 5 can be written as

$$\vec{F} = \int_{m_s} [\vec{a}_o + \dot{\vec{\omega}} \times \vec{r} + \vec{\omega} \times (\vec{\omega} \times \vec{r})]\, dm + 2\int_{m_g} \vec{\omega} \times \vec{V}_r\, dm + \int_{m_g} \vec{a}_r\, dm \tag{6}$$

and $$\vec{M} = \int_{m_s} \vec{r} \times [\vec{a}_o + \dot{\vec{\omega}} \times \vec{r} + \vec{\omega} \times (\vec{\omega} \times \vec{r})]\, dm +$$

$$2 \int_{m_g} \vec{r} \times (\vec{\omega} \times \vec{V}_r)\, dm + \int_{m_g} \vec{r} \times \vec{a}_r\, dm \qquad (7)$$

The first of the three integrals in Equations 6 and 7 will be referred to as rigid body integrals; the second, as jet damping integrals; and the third, as thrust integrals.

Rigid Body Integrals

Noting that $\vec{a}_o$, $\vec{\omega}$, and $\dot{\vec{\omega}}$ are common to all mass particles comprising m_s, the first integral in Equation 6 can be written as

$$\vec{A}_r = \vec{a}_o\, m_s + \dot{\vec{\omega}} \times \int_{m_s} \vec{r}\, dm + \vec{\omega} \times (\vec{\omega} \times \int_{m_s} \vec{r}\, dm) \qquad (8)$$

The integral in Equation 8 is equal to $m_s \vec{r}_c$ where the vector $\vec{r}_c$ describes the location of the center of gravity of the vehicle with respect to the origin of the body axes. The center of gravity of the vehicle will be restricted to lie on the X_B axis so the $\vec{r}_c = x_c \vec{i}$. Equation 8 can be expanded to read

$$\vec{A}_r = m_s [\vec{a}_{o_x} - (q^2 + r^2) X_c] \vec{i} + m_s [\vec{a}_{o_y} + (\dot{r} + pq) X_c] \vec{j} +$$

$$m_s [a_{o_z} - (\dot{q} - pr) X_c] \vec{k} \qquad (9)$$

The first integral in Equation 7 can be written as

$$\vec{G}_r = m_s \vec{r}_c \times \vec{a}_o + \int_{m_s} \vec{r} \times (\dot{\vec{\omega}} \times \vec{r})\, dm + \int_{m_s} \vec{r} \times [\vec{\omega} \times (\vec{\omega} \times \vec{r})]\, dm \qquad (10)$$

Imposing the requirement that the body axes are principal axes of inertia, Equation 10 can be expanded to yield

$$\vec{G}_r = [\dot{p}\, I_{x_s} + rq\,(I_{z_s} - I_{y_s})\,\vec{i} +$$

$$[\dot{q} I_{y_s} + rp\,(I_{x_s} - I_{z_s}) - m_s\, x_c\, a_{o_z}]\,\vec{j} +$$

$$[\dot{r} I_{z_s} + pq\,(I_{y_s} - I_{x_s}) + m_s\, x_c\, a_{o_y}]\,\vec{k} \qquad (11)$$

In some versions of this program $I_{y_s} = I_{z_s}$; however, since they are sometimes distinct, they will be designated separately. In some versions of this program the body axes are not principal axes, but in those cases, thrust must be zero and mass is constant.

Jet Damping Integrals

These integrals are the negative of the force and moment reactions applied to the vehicle by the Coriolis acceleration of the propellant gases prior to passage through the nozzle exit plane.

The jet damping force is related to the second integral in Equation 6 by the expression

$$\vec{F}_J = -2\int_{m_g} \vec{\omega} \times V_r\, dm = 2\,[\int_{m_g} (r\, V_{r_y} - q\, V_{r_z})\, dm]\,\vec{i} +$$

$$2\,[\int_{m_g} (p\, V_{r_z} - r\, V_{r_x})\, dm]\,\vec{j} + 2\,[\int_{m_g} (q\, V_{r_x} - p\, V_{r_y})\, dm]\,\vec{k} \qquad (12)$$

If the velocity field of the propellant gases is axisymmetric with respect to the X_B axis, then terms involving V_{r_y} and V_{r_z} drop out by cancellation when we integrate over opposite sides of the X_B axis and

$$\vec{F}_J = -J_1\,(r\,\vec{j} - q\,\vec{k}) \qquad (13)$$

where

$$J_1 = 2\int_{m_g} V_{r_x}\, dm$$

Similarly, the jet damping moment is given by the expression

$$\vec{M}_J = -2\int_{m_g} \vec{r} \times (\vec{\omega} \times \vec{V}_r)\, dm$$

$$= 2[\int_{m_g} (q\,y\,V_{r_x} + r\,z\,V_{r_x} - p\,y\,V_{r_y} - p\,z\,V_{r_z})\,dm]\,\vec{i} +$$

$$2[\int_{m_g} (r\,z\,V_{r_y} + p\,x\,V_{r_y} - q\,z\,V_{r_z} - q\,x\,V_{r_x})\,dm]\,\vec{j} +$$

$$2[\int_{m_g} (p\,x\,V_{r_z} + q\,y\,V_{r_z} - r\,x\,V_{r_x} - r\,y\,V_{r_y})\,dm]\,\vec{k} \qquad (14)$$

In addition to the assumption that the propellant gas flow is symmetric about the X_B axis, it is also assumed that the passage through which these gases flow has a sufficiently small diameter and curvature such that the approximations $x>>y$, $x>>z$, $V_{r_x} >> V_{r_y}$, and $V_{r_x} >> V_{r_z}$ can be made in Equation 14.

Therefore,

$$\vec{M}_J = -J_2\,(q\vec{j} + r\vec{k}) \qquad (15)$$

where

$$J_2 = 2\int_{m_g} x\,V_{r_x}\,dm$$

Thrust Integrals

The thrust integrals are the negative of the thrust forces and moments produced by the motor. These forces and moments account for the reactions due to the momentum flux of the propellant gases passing through the nozzle exit plane, plus the pressure acting on the nozzle exit area.

The thrust force is

$$\vec{F}_T = \int_{m_g} \vec{a}_r\, dm \qquad (16)$$

In general

$$\int_{m_g} \vec{a}_r \, dm = \int_{m_g} \frac{1}{\rho_g} \frac{\partial(\rho_g \vec{V}_r)}{\partial t} \, dm + \int_{A_e} (\mu_e \vec{V}_e - \vec{\pi}_e) da$$

where the first integral on the right side of this expression is a volume integral similar to others previously treated. The second integral is a surface integral evaluated over the nozzle exit surface. If the propellant gas flow is steady then the thrust force can be shown to be

$$\vec{F}_T = \int_{A_e} (\vec{\pi}_e - \mu_e \vec{V}_e) da \tag{17}$$

where

$$\vec{\pi}_e = (p_e - p) \vec{n}_e$$

and

$$\mu_e = -\rho_e (\vec{V}_e \cdot \vec{n}_e)$$

p_e, ρ_e, and $\vec{V}_e$ are the static pressure, density and velocity of the propellant gases at the nozzle exit plane; $\vec{n}_e$ is the unit inward normal to this plane; and p is the ambient atmospheric pressure. Assuming that p_e, ρ_e, $\vec{V}_e$, and $\vec{n}_e$ are constant over the nozzle exit plane, and that $\vec{V}_e$ and $\vec{n}_e$ are parallel at all points on this plane, then Equation 17 becomes

$$\vec{F}_T + (p_e - p) A_e \vec{n}_e + \vec{V}_e \int_{A_e} \rho_e (\vec{V}_e \cdot \vec{n}_e) da$$

Now note that

$$\int_{A_e} \rho_e (\vec{V}_e \cdot \vec{n}_e) da = \rho_e (\vec{V}_e \cdot \vec{n}_e) \int_{A_e} da = \dot{m} < o$$

and also that

$$\vec{V}_e = -V_e \vec{n}_e$$

so that

$$\vec{F}_T = T \vec{n}_e$$

where

$$T = [(p_e - p)A_e - \dot{m} V_e]$$

The orientation of the unit vector $\vec{n}_e$ with respect to the body frame is shown below:

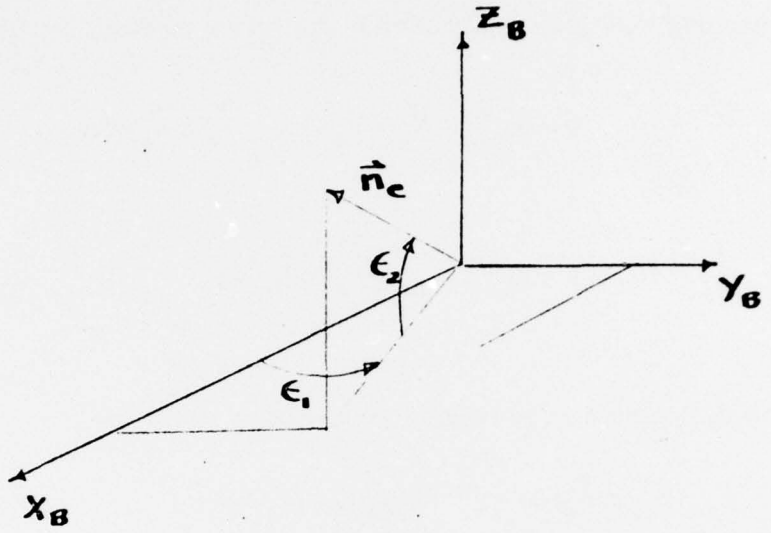

The vector $\vec{n}_e$ in the body frame can be written as

$$\vec{n}_e = \cos(\varepsilon_2)\ \cos(\varepsilon_1)\ \vec{i} + \cos(\varepsilon_2)\ \sin(\varepsilon_1)\ \vec{j} + \sin(\varepsilon_2)\ \vec{k}$$

If the angles ε_1 and ε_2 are sufficiently small then

$$\vec{F}_T = T\ (\vec{i} + \varepsilon_1\ \vec{j} + \varepsilon_2\ \vec{k}) \tag{18}$$

The thrust moment is

$$\vec{M}_T = -\int_{m_g} \vec{r} \times \vec{a}_r\ dm \tag{19}$$

For the case where the propellant gas flow is steady, similar to the case of thrust force, Equation 19 can be written as

$$\vec{M}_T = \int_{A_e} \vec{r}_e \times (\vec{\pi}_e - \mu_e \vec{V}_e)\, da \tag{20}$$

where $\vec{r}_e$ is the position vector of any point on the exhaust exit plane. Under the assumptions previously stated, the thrust moment can be written as

$$\vec{M}_T = [p_e - p - \rho_e V_e (\vec{V}_e \cdot \vec{n}_e)] \int_{A_e} (\vec{r}_e \times \vec{n}_e)\, da$$

or simply

$$\vec{M}_T = (p_e - p + \rho_e V_e^2) \int_{A_e} (\vec{r}_e \times \vec{n}_e)\, da \tag{21}$$

The integral in Equation 21 is readily expanded to yield

$$\int_{A_e} (\vec{r}_e \times \vec{n}_e)\, da = \int_{A_e} [(y_e \varepsilon_2 - z_e \varepsilon_1)\, \vec{i} +$$

$$(z_e - x_e \varepsilon_2)\, \vec{j} + (x_e \varepsilon_1 - y_e)\, \vec{k}]\, da$$

resulting in the expression

$$\vec{M}_T = T [(\varepsilon_2 \hat{y}_e - \varepsilon_1 \hat{z}_e)\, \vec{i} + (\hat{z}_e - \hat{x}_e \varepsilon_2)\, \vec{j} + (\bar{x}_e \varepsilon_1 - \hat{y}_e)\, \vec{k}] \tag{22}$$

where

$$\int_{A_e} X_e\, da = \hat{X}_e A_e, \text{ etc}$$

so that $\hat{X}_e$, $\hat{y}_e$, $\hat{z}_e$ are the coordinates of the centroid of A_e measured in the body frame.

Gravity Forces and Moments

The gravity force is given by the expression

$$\vec{F}_G = - g_o R_E^2 \int \frac{\hat{R}}{|\hat{R}|^3} \, dm \tag{23}$$

where $\hat{R}$ is the position vector of an infinitesmal mass (dm) of the vehicle with respect to the Earth's center. For a vehicle of reasonably small dimensions, flying in the atmosphere, a good approximation is

$$\hat{R} \approx \vec{R}$$

where $\bar{R}$ is the position vector of the center of gravity of the vehicle with respect to the Earth's center. Neglecting the effect of gravity on the propellant gas particles, then

$$\vec{F}_G = \frac{- m_s g_o R_E^2}{|\vec{R}|^3} (x_o \vec{i} + y_o \vec{j} + z_o \vec{k}) \tag{24}$$

where x_o, y_o, z_o are the components of $\vec{R}$ in the body frame.

The gravity moment is given by the expression

$$\vec{M}_G = g_o R_e^2 \int \frac{\hat{R} \times \vec{r}}{|\hat{R}|^3} \, dm \tag{25}$$

Again, assuming that $\hat{R} \approx R$ Equation 25 becomes

$$\vec{M}_G = \frac{g_o R_E^2}{|\vec{R}|^3} \int (\vec{R} \times \vec{r}) \, dm = \frac{g_o R_E^2}{|\vec{R}|^3} \vec{R} \times \int \vec{r} \, dm$$

Neglecting the mass of the propellant gases and recalling that

$$\int_{m_s} \vec{r} \, dm = m_s \vec{r}_c = m_s x_c \vec{i}$$

the gravity moment can be written as

$$\vec{M}_G = \frac{m_s g_o R_E^2}{|\vec{R}|^3} x_c (z_o \vec{j} - y_o \vec{k}) \tag{26}$$

Aerodynamic Forces and Moments

The aerodynamic forces and moments acting on the vehicle can be written as

$$\vec{F}_A = QA (C_X \vec{i} + C_Y \vec{j} + C_Z \vec{k}) \tag{27}$$

and

$$\vec{M}_A = QAd (C_L \vec{i} + C_M \vec{j} + C_N \vec{k}) \tag{28}$$

These equations will be developed in more detail in a subsequent section.

Substituting the definitions of $\vec{A}_r$ from Equation 8, $\vec{F}_J$ from Equation 12, $\vec{F}_T$ from Equation 16, $\vec{F}_G$ from Equation 23 and $\vec{F}_A$ from Equation 27 into Equation 6 we get

$$\vec{A}_r = \vec{F}_G + \vec{F}_A + \vec{F}_T + \vec{F}_J$$

Similarly the definitions of $\vec{G}_r$ from Equation 10, $\vec{M}_J$ from Equation 14, $\vec{M}_T$ from Equation 19, $\vec{M}_G$ from Equation 25 and $\vec{M}_A$ from Equation 28, substituted into Equation 7 yield

$$\vec{G}_r = \vec{M}_G + \vec{M}_A + \vec{M}_T + \vec{M}_J$$

Expanding the forces and accelerations above and rearranging the terms, we get

$$\begin{bmatrix} a_{o_x} \\ a_{o_y} \\ a_{o_x} \end{bmatrix} = -\frac{g_o R_E^2}{|\vec{R}|^3} \begin{bmatrix} x_o \\ y_o \\ z_o \end{bmatrix} + \frac{1}{m_s} \begin{bmatrix} F_x \\ F_y \\ F_z \end{bmatrix} + \frac{T}{m_s} \begin{bmatrix} 1 \\ \varepsilon_1 \\ \varepsilon_2 \end{bmatrix}$$

$$- \frac{J_1}{m_s} \begin{bmatrix} o \\ r \\ -q \end{bmatrix} + x_c \begin{bmatrix} q^2 + r^2 \\ -\dot{r} - pq \\ \dot{q} - pr \end{bmatrix} \tag{29}$$

and

$$\begin{bmatrix} \dot{p}\, I_{x_s} + rq(I_{z_s} - I_{y_s}) \\ \dot{q}\, I_{y_s} + rp(I_{x_s} - I_{z_s}) \\ \dot{r}\, I_{z_s} + pq(I_{y_s} - I_{x_s}) \end{bmatrix} = \frac{m_s g_o R_E^2 x_c}{|\vec{R}|^3} \begin{bmatrix} 0 \\ z_o \\ -y_o \end{bmatrix} + \begin{bmatrix} M_x \\ M_y \\ M_z \end{bmatrix}$$

$$+ T \begin{bmatrix} \varepsilon_2\, \hat{y}_e - \varepsilon_1\, \hat{z}_e \\ \hat{z}_e - \hat{x}_e\, \varepsilon_2 \\ \hat{x}_e\, \varepsilon_1 - \hat{y}_e \end{bmatrix} - J_2 \begin{bmatrix} o \\ q \\ r \end{bmatrix} + m_s x_e \begin{bmatrix} o \\ a_{o_z} \\ -a_{o_y} \end{bmatrix} \tag{30}$$

where

$$\begin{bmatrix} F_x \\ F_y \\ F_z \end{bmatrix} = QA \begin{bmatrix} C_X \\ C_Y \\ C_Z \end{bmatrix}$$

and

$$\begin{bmatrix} M_x \\ M_y \\ M_z \end{bmatrix} = QAd \begin{bmatrix} C_L \\ C_M \\ C_N \end{bmatrix}$$

The force Equation 29 will now be written in terms of inertial frame components. The transformation matrix $[\ell_B]$ transforms vector components in the body frame to vector components in the inertial frame. The components of the vectors $\vec{a}_o$ and $\vec{R}$ in these two frames are, therefore, related by the expressions

$$\begin{bmatrix} a_{o_x} \\ a_{o_y} \\ a_{o_z} \end{bmatrix} = [\ell_B]^T \begin{bmatrix} \ddot{X}_R \\ \ddot{Y}_R \\ \ddot{Z}_R \end{bmatrix}$$

and

$$\begin{bmatrix} x_o \\ y_o \\ z_o \end{bmatrix} = [\ell_B]^T \begin{bmatrix} X_R \\ Y_R \\ Z_R \end{bmatrix}$$

Note that $\vec{a}_o$ was the acceleration of the origin of the body frame with respect to an inertial coordinate system instantaneously parallel with the body frame.

Substituting these expressions into Equation 29 and premultiplying each side by $[\ell_B]$, the force equation becomes

$$\begin{bmatrix} \ddot{X}_R \\ \ddot{Y}_R \\ \ddot{Z}_R \end{bmatrix} = -\frac{g_o R_E^2}{|\vec{R}|^3} \begin{bmatrix} X_R \\ Y_R \\ Z_R \end{bmatrix} +$$

$$[\ell_B] \left\{ \frac{1}{m_s} \begin{bmatrix} F_x \\ F_y \\ F_z \end{bmatrix} + \frac{T}{m_s} \begin{bmatrix} 1 \\ \varepsilon_1 \\ \varepsilon_2 \end{bmatrix} - \frac{J_1}{M_s} \begin{bmatrix} o \\ r \\ -q \end{bmatrix} + x_c \begin{bmatrix} q^2 + r^2 \\ -\dot{r} - pq \\ \dot{q} - pr \end{bmatrix} \right\} \quad (31)$$

Equations 30 and 31 now will be written in a form which will allow the use of a body frame rigidly attached to the vehicle, for which they are already valid, or for a body frame which does not roll with the missile. The necessary transformations of the Force Equation 31 and the Moment Equation 30 will be presented next.

Symbolically, Equation 31 can be written as

$$\vec{P} = \vec{F}_G + [\ell_B] \{ \vec{F}_A + \vec{F}_T + \vec{F}_J + \vec{F}_I \}$$

The vectors $\vec{P}$ and $\vec{F}_G$, which describe the inertial acceleration of the body axes origin and the gravity forces, are already in the desired form since they are described in terms of variables resolved in the inertial frame.

The matrix $[\ell_B]$ can be calculated so that it will transform a vector in either a rolling or nonrolling body frame into a vector in the inertial frame. This is shown in Reference 1 and repeated here for convenience. The $[\ell_B]$ matrix is calculated by integrating the set of nine differential equations

$$[\dot{\ell}_B] = [\ell_B] [\Omega]$$

where

$$[\Omega] = \begin{bmatrix} o & -r & q \\ r & 0 & -kp \\ -q & kp & o \end{bmatrix}$$

If k = 1 the body axes are rolling, and if k = 0 they are nonrolling. A correction procedure for the minimization of the nonorthogonality introduced by the numerical integration of these equations is incorporated.

The calculation of the aerodynamic force vector $\vec{F}_A$, as will be seen later, is accomplished in such a way that either the rolling or nonrolling computational frames can be used. The thrust $\vec{F}_T$, jet damping $\vec{F}_J$ and inertia $\vec{F}_I$ force vectors now must be transformed.

The orientation of the rolling frame (x, y, z) with respect to the rolling or nonrolling computational frame (x′, y′, x′) is depicted in the sketch below.

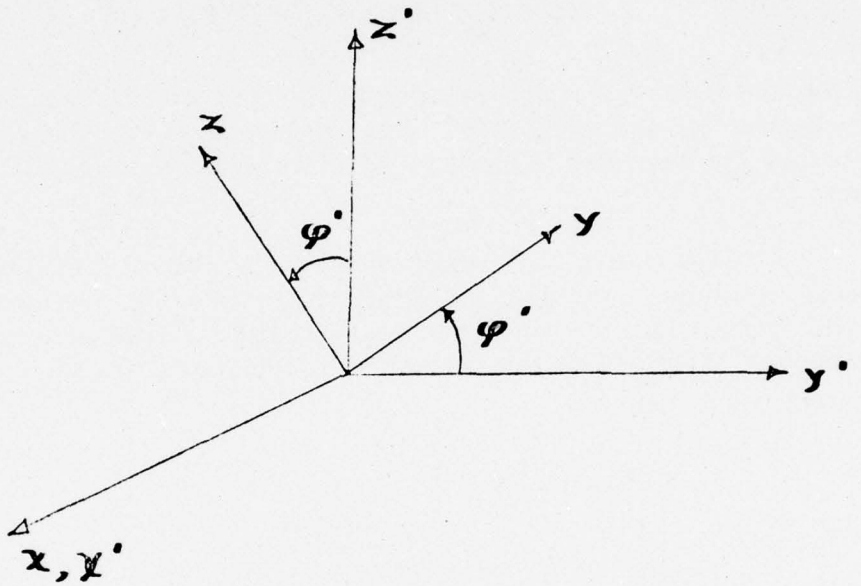

The components of any vector in the rolling or nonrolling computational frame are related to its components in the rolling, body-fixed frame by the expression

$$\vec{V} = [\ell\varphi'] \vec{V}'$$

where primes denote vectors resolved in the computational frame.

The components of the time rate of change of $\vec{V}$ are given by

$$\dot{\vec{V}} = [\ell\dot{\varphi}'] \vec{V}' + [\ell\varphi'] \dot{\vec{V}}'$$

where

$$[\ell\varphi'] = \begin{bmatrix} 1 & o & o \\ o & \cos\varphi' & \sin\varphi' \\ o & -\sin\varphi' & \cos\varphi' \end{bmatrix}$$

Using these relations, the vectors $\vec{F}_T$, $\vec{F}_J$ and $\vec{F}_I$ transform

$$\vec{F}_T' = [\ell\varphi']^T \vec{F}_T = \frac{T}{m_s} \begin{bmatrix} 1 \\ \varepsilon_1 \cos(\varphi') - \varepsilon_2 \sin(\varphi') \\ \varepsilon_2 \cos(\varphi') + \varepsilon_1 \sin(\varphi') \end{bmatrix}$$

$$\vec{F}_J' = [\ell\varphi]^T \vec{F}_J = -\frac{J_1}{m_s} \begin{bmatrix} o \\ r' \\ -q' \end{bmatrix}$$

where

and

$$r' = r\cos(\varphi') + q\sin(\varphi')$$

$$q' = q\cos(\varphi') - r\sin(\varphi')$$

$$\vec{F}_I' = [\ell\varphi']^T \vec{F}_I = x_c \begin{bmatrix} q'^2 + r'^2 \\ -\dot{r}' \\ \dot{q}' \end{bmatrix}$$

where

$$\dot{r}' = [\dot{r} + q\ (1-k)p]\cos(\varphi') + [q - r\,(1-k)p]\sin(\varphi')$$

and

$$\dot{q}' = [\dot{q} - r\ (1-k)p]\cos(\varphi') - [\dot{r} + q\,(1-k)p]\sin(\varphi')$$

Since the roll angle φ' is determined from the differential equation

$$\dot{\varphi}' = (1-k)p$$

with initial condition

$$\varphi'(o) = o$$

Equation 31 can now be written in a form which applies to either a rolling or nonrolling computational frame, depending upon the choice of k. That is,

$$\begin{bmatrix} \ddot{X}_R \\ \ddot{Y}_R \\ \ddot{Z}_R \end{bmatrix} = -\frac{g_o R_E^2}{|\vec{R}|^3} \begin{bmatrix} X_R \\ Y_R \\ Z_R \end{bmatrix} + [\ell_B] \left\{ \frac{1}{m_s} \begin{bmatrix} F_x \\ F_y \\ F_z \end{bmatrix} + \right.$$

$$\left. \frac{T}{m_s} \begin{bmatrix} 1 \\ \varepsilon_1 \cos(\varphi') - \varepsilon_2 \sin(\varphi') \\ \varepsilon_2 \cos(\varphi') + \varepsilon_1 \sin(\varphi') \end{bmatrix} - \frac{J_1}{m_s} \begin{bmatrix} o \\ r \\ -q \end{bmatrix} + x_c \begin{bmatrix} q^2 + r^2 \\ -\dot{r} - kpq \\ \dot{q} - kpr \end{bmatrix} \right\} \tag{36}$$

The primes on the angular velocities are dropped since it is understood that these variables are measured in the particular frame which is being used for computation.

The transformation of Equation 30 is accomplished in a similar fashion; the symbolic form of this equation is

$$\vec{H} = \vec{M}_G + \vec{M}_A + \vec{M}_T + \vec{M}_J + \vec{M}_I$$

Writing the rate of change of angular momentum in the computational frame, which may be rolling or nonrolling, we get

$$\vec{H} = \begin{bmatrix} \dot{p} I_{x_s} \\ \dot{q} I_{y_s} \\ \dot{r} I_{z_s} \end{bmatrix} + [\Omega] \begin{bmatrix} p I_{x_s} \\ q I_{y_s} \\ r I_{z_s} \end{bmatrix}$$

It should be pointed out that this form is good only for those cases where $I_{y_s} = I_{z_s}$. The vector $\vec{H}$ could easily be put in a form compatible with both the rolling and nonrolling frames for the case where $I_{y_s} \neq I_{z_s}$, but some of the advantage of using the nonrolling frame would be lost, since the moment of inertia matrix would not be constant in the nonrolling computational frame and an additional term would have to be calculated. Furthermore, the computation of the moment of inertia and its rate of change would then require an accurate knowledge of the roll position of the body fixed axes, precisely what we are trying to avoid computing by introducing the nonrolling computational axes.

As in the case of the aerodynamic forces, the vector $\vec{M}_A$ will be calculated in a manner compatible with both the rolling and nonrolling frames. The gravity, thrust, jet damping, and inertia moment vectors are transformed as were the force vectors.

Using Equation 33, the transformed vectors are

$$\vec{M}_G' = \frac{m_s g_o R_E^2 x_c}{|\vec{R}|^3} \begin{bmatrix} o \\ z_o' \\ -y_o' \end{bmatrix}$$

$$\vec{M}_T' = T \begin{bmatrix} \varepsilon_2 \hat{y}_e - \varepsilon_1 \hat{z}_e \\ (z_e - \varepsilon_2 \hat{x}_e) \cos(\varphi') - (\varepsilon_1 \hat{x}_e - \hat{y}_e) \sin(\varphi') \\ (\varepsilon_1 \hat{x}_e - \hat{y}_e) \cos(\varphi') + (\hat{z}_e - \varepsilon_2 \hat{x}_e) \sin(\varphi') \end{bmatrix}$$

$$\vec{M}_J' = -J_2 \begin{bmatrix} o \\ q' \\ r' \end{bmatrix}$$

$$\vec{M}_I' = m_s x_c \begin{bmatrix} o \\ a'_{o_z} \\ -a'_{o_y} \end{bmatrix}$$

so that the moment equation becomes

$$\begin{bmatrix} \dot{p} I_{x_s} \\ \dot{q} I_{y_s} \\ \dot{r} I_{z_s} \end{bmatrix} = - [\Omega] \begin{bmatrix} pI_{x_s} \\ qI_{y_s} \\ rI_{z_s} \end{bmatrix} + \frac{m_s g_o R_E^2 x_c}{|\vec{R}|^3} \begin{bmatrix} o \\ z_o \\ -y_o \end{bmatrix} +$$

$$\begin{bmatrix} M_x \\ M_y \\ M_z \end{bmatrix} + T \begin{bmatrix} \varepsilon_2 \hat{y}_e - \varepsilon_1 \hat{z}_e \\ (\hat{z}_e - \varepsilon_2 \hat{x}_e) \cos(\varphi') - (\varepsilon_1 \hat{x}_e - \hat{y}_e) \sin(\varphi') \\ (\varepsilon_1 \hat{x}_e - \hat{y}_e) \cos(\varphi') + (\hat{z}_e - \varepsilon_2 \hat{x}_e) \sin(\varphi') \end{bmatrix}$$

$$- J_2 \begin{bmatrix} o \\ q \\ r \end{bmatrix} + m_s x_c \begin{bmatrix} o \\ a_{o_z} \\ -a_{o_y} \end{bmatrix} \qquad (37)$$

Differential Equations 36 and 37 describe the motion of a rolling or nonrolling computational frame which has its origin fixed at the burnout center of gravity of the vehicle. These equations are not in a form suitable for integration because of the terms $\dot{r}$ and $\dot{q}$ in Equation 36, and a_{o_y} and a_{o_x} in Equation 37.

At this point it should be recalled that in order to calculate the aerodynamic forces and moments, the velocity of the vehicle structure with respect to the local air mass must be known. However, the velocity of the origin of the body frame is not the same as this velocity because of the rotational acceleration components which account for the fact that the

burnout center of gravity position does not coincide with the instantaneous center of gravity position. If the last term in Equation 36 is suppressed, then these equations describe the position of the instantaneous center of gravity and the velocity of a fixed point coinciding with the instantaneous center of gravity at any given time.

The Moment Equation, 37, can be readily put into a form suitable for integration if Equation 29 is used to eliminate a_{o_y} and a_{o_z} and if the remaining inertia terms are transformed so that they are compatible with both computational frames.

The force and moment equations can now be written, in their final form:

$$\begin{bmatrix} \ddot{X}_R \\ \ddot{Y}_R \\ \ddot{Z}_R \end{bmatrix} = -\frac{g_o R_E^2}{|\vec{R}|^3} \begin{bmatrix} X_R \\ Y_R \\ Z_R \end{bmatrix} + [\ell_B] \left\{ \frac{1}{M_s} \begin{bmatrix} F_x \\ F_y \\ F_z \end{bmatrix} + \frac{T}{M_s} \begin{bmatrix} 1 \\ \varepsilon_1 \cos(\varphi') - \varepsilon_2 \sin(\varphi') \\ \varepsilon_2 \cos(\varphi') + \varepsilon_1 \sin(\varphi') \end{bmatrix} - \frac{J_1}{m_s} \begin{bmatrix} o \\ r \\ -q \end{bmatrix} \right\} \quad (38)$$

$$\begin{bmatrix} p\, I_{x_s} \\ \dot{q}\,(I_{y_s} - m_s x_c^2) \\ \dot{r}\,(I_{z_s} - m_s x_c^2) \end{bmatrix} = -[\Omega] \begin{bmatrix} p\,(I_{x_s} + k\, m_s x_c^2) \\ q\, I_{y_s} \\ r\, I_{z_s} \end{bmatrix} + \begin{bmatrix} M_x \\ M_y \\ M_z \end{bmatrix} +$$

$$T \begin{bmatrix} \varepsilon_2 \hat{y}_e - \varepsilon_1 \hat{z}_e \\ (\hat{z}_e - \varepsilon_2 \hat{x}_e) \cos(\varphi') - (\varepsilon_1 \hat{x}_e - \hat{y}_e) \sin(\varphi') \\ (\varepsilon_1 \hat{x}_e - \hat{y}_e) \cos(\varphi') + (\hat{z}_e - \varepsilon_2 \hat{x}_e) \sin(\varphi') \end{bmatrix}$$

$$- J_2 \begin{bmatrix} o \\ q \\ r \end{bmatrix} \qquad (39)$$

Since Equation 38 can be simply transformed to a set of six first order differential equations, Equations 32, 35, 38, and 39 are equivalent to a set of nineteen first-order differential equations describing the vehicle's motion.

Equations Describing Physical Characteristics of Vehicle

The physical characteristics of the vehicle are calculated based on two models of the rocket motor. Both have a single period during which thrust occurs, and both have constant mass flow rate during burning with ignition occurring at $t = t_1$ and burnout occurring at $t = t_2$. Two sets of equations are presented: one for an end burning grain, and the other for a radially burning grain.

The calculations of thrust and mass are identical for both cases. The thrust equation is

$$T = [(p_e - p) A_e - \dot{m} V_e]$$

All quantities except the ambient atmospheric pressure (p) are input constants. The ambient pressure is a function of altitude as given in Reference 3. The instantaneous vehicle mass and propellant mass are

$$m_s = m + m_p$$

and

$$m_p = m_{p_o} + \dot{m} (t - t_1)$$

All quantities except t are input constants, with m being a negative quantity.

The remainder of the calculations depend on the mode of burning and will be considered in two parts. Refer to Figure 1 for a sketch showing the dimensions involved.

End Burning Grain

1. Center of gravity location:

$$x_c = \frac{m_p}{m_s} x_2$$

2. Axial moment of inertia:

$$I_{x_s} = I_x + \frac{m_p r_1^2}{2}$$

3. Transverse moment of inertia:

$$I_{y_s} = I_{z_s} = I_y + m_p \left[\frac{r_1^2}{4} + \frac{(x_1 - x_3)^2}{12} + x_2^2 \right]$$

4. Jet damping factors:

$$J_1 = 2\int_{m_g} V_{r_x} \, dm = 2\iint \rho_g V_{r_x} \, da \, dx$$

$$J_1 = 2\dot{m}\int_{x_4}^{x_3} dx = 2\dot{m}(x_3 - x_4)$$

Similarly

$$J_2 = 2\int_{m_g} x V_{r_x} \, dm = \dot{m}(x_3^2 - x_4^2)$$

For this case, x_1, x_4, and r_1 are input constants and

$$x_2 = \frac{1}{2}(x_1 + x_3)$$

$$x_3 = x_{3_o} - \frac{\dot{m}\,(t - t_1)}{\pi\, r_1^{\,2}\, \rho_p}$$

Radially Burning Grain

1. Center of gravity location:

$$x_c = \frac{m_p}{m_s}\, x_2$$

2. Axial moment of inertia:

$$I_{x_s} = I_x + \frac{m_p}{2}(r_1^{\,2} + r_2^{\,2})$$

3. Transverse moment of inertia:

$$I_{y_s} = I_{z_s} = I_y + m_p\left[\frac{r_1^{\,2} + r_2^{\,2}}{4} + \frac{(x_1 - x_3)^2 + x_2^{\,2}}{12}\right]$$

4. Jet damping factors:

$$J_1 = 2\int\int \rho_g\, V_{r_x}\, da\, dx$$

In this case, however,

$$\int \rho_g\, V_{r_x}\, da = \begin{cases} \dot{m}\,\dfrac{x - x_1}{x_3 - x_1} & x_1 \geq x > x_3 \\ \dot{m} & x_3 \geq x \geq x_4 \end{cases}$$

So that

$$J_1 = 2\int_{x_3}^{x_1} \dot{m} \left(\frac{x - x_1}{x_3 - x_1}\right) dx + 2\int_{x_4}^{x_3} \dot{m}\, dx$$

$$J_1 = \dot{m}\,(x_1 + x_3 - 2\,x_4)$$

Similarly,

$$J_2 = 2\int\int x\, \rho_g\, V_{r_x}\, d\,a\, d\,x$$

$$J_2 = \frac{m}{3}(x_1^{\,2} + x_3^{\,2} + x_1\, x_3 - 3\, x_4^{\,2})$$

For this case x_1, $x_2 = x_{2_o}$, $x_3 = x_{3_o}$, x_4, and r_1 are input constants and

$$r_2 = \sqrt{r_{2_o}^{\,2} - \frac{\dot{m}\,(t - t_1)}{\pi\, \rho_p\, (x_1 - x_3)}}$$

Reference 5 contains additional information on the calculation of the jet damping factors.

AERODYNAMIC FORCE AND MOMENT EQUATIONS

The aerodynamic forces and moments as input to the program are always calculated as originating in their proper coordinate system; i.e., the trim normal force, $F_{z_{\delta_A}}$, is resolved into body fixed coordinates no matter whether integration takes place in body fixed or nonrolling coordinates. The computational frame, subscripted AB, into which all aerodynamic forces and moments are resolved is shown on Figure 2. The following roll position and roll relationship angles are needed for the analysis:

ϕ Azimuth angle of the angle of attack plane in the AB frame

φ' Roll angle between AB frame and rolling, body-fixed frame

φ Azimuth angle of the angle of attack plane in the rolling, body-fixed plane

ϕ' Reduced φ; it is [φ Modulo ξ] where ξ is the repeat roll angle of the aerodynamic symmetry

The total aerodynamic force and moment coefficients, in terms of the Taylor series expansion coefficients, are

$$C_X \equiv C_x + C_{x_p} \left(\frac{pd}{2V_A}\right) \qquad \text{(for a normal missile } C_X < o\text{)}$$

$$C_Y \equiv C_y \cos(\phi) + C_z \sin(\phi) + C_{y_p} \left(\frac{pd}{2V_A}\right) \cos(\phi) + C_{z_{\delta_A}} [\delta_B \cos(\varphi') - \delta_A \sin(\varphi')]$$

(for a normal missile if $\phi < 90°$, $C_Y < o$)

$$C_Z \equiv C_z \cos(\phi) - C_y \sin(\phi) - C_{y_p} \left(\frac{pd}{2V_A}\right) \sin(\phi) + C_{z_{\delta_A}} [\delta_A \cos(\varphi') + \delta_B \sin(\varphi')]$$

(for a normal missile $C_Z = o$ by the axisymetric assumption)

$$C_L \equiv C_\iota + C_{\iota_\delta} \delta + C_{\iota_p} \left(\frac{pd}{2V_A}\right)$$

$$C_M \equiv C_m \cos(\phi) + C_n \sin(\phi) + C_{n_p} \left(\frac{pd}{2V_A}\right) \sin(\phi) + C_{m_q} \left(\frac{qd}{2V_A}\right) + C_{m_{\delta_A}} [\delta_A \cos(\varphi') - \delta_B \sin(\varphi')]$$

(for a statically stable missile, $C_m = < o$)

$$C_N \equiv C_n \cos(\phi) - C_m \sin(\phi) + C_{n_p} \left(\frac{pd}{2V_A}\right) \cos(\phi) + C_{m_q} \left(\frac{rd}{2V_A}\right) +$$

$$C_{m_{\delta_A}} [\delta_B \cos(\varphi') + \delta_A \sin(\varphi')] \qquad (40)$$

(for a normal missile, $C_n = o$ by the axisymmetric assumption)

where C_x, C_{x_p}, C_{y_p}, $C_{z_{\delta_A}}$, C_{l_δ}, C_{l_p}, C_{m_q}, C_{n_p}, and $C_{m_{\delta_A}}$ are functions of Mach number and total angle of attack. The coefficients C_y, C_z, C_l, C_m and C_n are functions of Mach number, total angle of attack, and reduced azimuth angle of the angle of attack plane, ϕ'.

AERODYNAMIC ORIENTATION ANGLES

In this section the aerodynamic orientation angles required for the calculation of the force and moment coefficients given in Equation 40 are defined. The angle of attack, sideslip, and total angle of attack are shown in Figure 2. It should be noted that, for a given orientation of the body with respect to the velocity vector, the values of α and β depend upon whether the body axes are rolling or nonrolling. The value of $\bar{\alpha}$, however, is independent of the choice of body axes. Also note that $\vec{V}_A$ and $\bar{\alpha}$ always lie in the $x_A - z_A$ plane.

$$\alpha = \text{Arctan} \left(\frac{V_{z_{BA}}}{V_{x_{BA}}} \right) \quad 180° \geq \alpha \geq -180° \qquad (41)$$

Range of α	Sign of $V_{z_{BA}}$	Sign of $V_{x_{BA}}$
$90° > \alpha > o°$	+	+
$180° > \alpha > 90°$	+	-
$0° > \alpha > -90°$	-	+
$-90° > \alpha > -180°$	-	-
$\alpha = o$	0	0

$$\beta = \text{Arctan}\left(\frac{V_{y_{BA}}}{V_{x_{BA}}}\right) \qquad 180° \geq \beta \geq -180° \qquad (42)$$

with the same sign conventions and quadrants as α

$$\bar{\alpha} = \text{Arctan}\left[\frac{\sqrt{V_{y_{BA}}^2 + V_{z_{BA}}^2}}{V_{x_{BA}}}\right] \qquad 180° \geq \bar{\alpha} \geq 0° \qquad (43)$$

Range of $\bar{\alpha}$	Sign of $V_{x_{BA}}$	Sign of $V_{y_{BA}}$	Sign of $V_{z_{BA}}$
$90° > \bar{\alpha} > 0°$	+	$\neq 0$	$\neq 0$
$180° > \bar{\alpha} > 90°$	-	$\neq 0$	$\neq 0$
$\bar{\alpha} = 0$	0	0	0

The roll angle ϕ, as is the case with α and β depends upon whether or not the body frame is rolling

$$\phi = \text{Arctan}\left(\frac{V_{y_{BA}}}{V_{z_{BA}}}\right) \qquad 360° > \phi \geq 0° \qquad (44)$$

Range of ϕ	Sign of $V_{y_{BA}}$	Sign of $V_{z_{BA}}$
$90° > \phi > 0°$	+	+
$180° > \phi > 90°$	+	-
$270° > \phi > 180°$	-	-
$360° > \phi > 270°$	-	+
$\phi = 0$	0	0

Initially, the rolling and nonrolling body frames are coincident. If it is desired to compute in a nonrolling frame when there is a configurational asymmetry reflected in a body-fixed force or moment, then the precise roll position of the actual body must be computed. The differential equation describing the roll relationship between the AB (rolling or nonrolling computational frame) and the body-fixed frame is Equation 35, reproduced here:

$$\dot{\varphi}' = (1 - k)p$$

However, this procedure is not particularly recommended since the point of introducing the nonrolling computational frame is to make it unnecessary to calculate the roll angle of the body-fixed frame accurately; if an asymmetry must be introduced in the body-fixed frame, its position must be accurately known. In any case, whether the roll position is known accurately or not, there exists a relationship among the roll angles: the azimuthal position of the angle of attack plane in the body-fixed frame is equal to azimuthal position of the angle of attack plane in the rolling or nonrolling computational frame plus the roll angle between the rolling or nonrolling computational frame and the rolling, body-fixed frame:

$$\varphi = \phi + \varphi' \tag{45}$$

Obviously, when $k = 1$, $\dot{\varphi}' = o$. Therefore $\varphi' = o$ and the AB frame *is identical with the body-fixed frame.*

As an example of the use of roll symmetry in the calculation of aerodynamic coefficients, consider a cruciform finned body. For such a body, the coefficients which are functions of roll angle (C_y, C_z, C_l, C_m, and C_n) are input from zero to 90° only, since these coefficients repeat their values over each 90° of roll. From (the true azimuthal angle of the angle of attack plane in the rolling, body-fixed axes) φ, we calculate a ficticious roll angle ϕ' (the reduced roll angle).

$$\phi' = \varphi \qquad 90° \geq \varphi \geq 0°$$

$$\phi' = \varphi - 90° \qquad 180° \geq \varphi > 90°$$

$$\phi' = \varphi - 180° \qquad 270° \geq \varphi > 180°$$

$$\phi' = \varphi - 210° \qquad 360° \geq \varphi > 210°$$

If the roll dependent coefficients repeat every 180°, the reduced roll angle is

$$\phi' = \varphi \qquad 180° \geq \varphi \geq 0°$$
$$\phi' = \varphi - 180° \qquad 360° \geq \varphi > 180°$$

Provision is made for a repeat angle of 60°, typical of a six-finned projectile, thus:

$$\phi' = \varphi \qquad 60° \geq \varphi \geq 0°$$
$$\phi' = \varphi - 60° \qquad 120° \geq \varphi > 60°$$
$$\phi' = \varphi - 120° \qquad 180° \geq \varphi > 120°$$
$$\phi' = \varphi - 180° \qquad 240° \geq \varphi > 180°$$
$$\phi' = \varphi - 240° \qquad 300° \geq \varphi > 240°$$
$$\phi' = \varphi - 300° \qquad 360° \geq \varphi > 300°$$

All other cases require that the roll dependence be supplied from 0° to 360°, and therefore

$$\phi' = \varphi$$

for all values of φ.

In all cases the table look-up and interpolation is performed with ϕ'as the independent variable for roll angle dependence.

ROUTINE INTERMEDIATE VARIABLE CALCULATIONS

The operation of the program requires regular calculations of dynamic pressure, Mach number, velocity of the air frame with respect to the local air mass, and other quantities from the fundamental variables X_R, Y_R, Z_R, their derivatives, and the Matrix $[\ell_B]$. We define a local axis system x_{LE}, y_{LE}, z_{LE}, see Figure 3, such that its origin is at the burnout center of mass of the body, its x_{LE} axis pointing North; its z_{LE} axis points East, and its y_{LE} axis points directly away from the center of the spherical Earth. Its location on the Earth is defined by its north latitude, ψ_R and its east longitude τ_R.

The components of the velocity of the body with respect to the Earth, in components along the local axes (subscripted LE) are

$$\begin{bmatrix} V_{x_{LE}} \\ V_{y_{LE}} \\ V_{z_{LE}} \end{bmatrix} = [\ell_L] \begin{bmatrix} \dot{X}_R \\ \dot{Y}_R \\ \dot{Z}_R \end{bmatrix} - \begin{bmatrix} 0 \\ 0 \\ \omega_E \sqrt{y_R^2 + z_R^2} \end{bmatrix} \tag{46}$$

where

$$[\ell_L] = \begin{bmatrix} \cos(\psi_R) & -\sin(\psi_R)\cos(\tau_R) & -\sin(\psi_R)\sin(\tau_R) \\ \sin(\psi_R) & \cos(\psi_R)\cos(\tau_R) & \cos(\psi_R)\sin(\tau_R) \\ 0 & -\sin(\tau_R) & \cos(\tau_R) \end{bmatrix}$$

and ω_E is the spin of the Earth and y_R and z_R are the equatorial components of the position of the burnout center of mass in inertial coordinates.

The angles τ_R and ψ_R are simply related to the components of the position vector:

$$\tau_R = \text{ARCTAN}\ (z_R/y_R) \qquad 360° > \tau_R \geq 0° \tag{47}$$

The usual quadrant assignment for τ_R is followed as a function of the signs of Z_R and Y_R:

Range of τ_R	Sign of Z_R	Sign of Y_R
$90° > \tau_R > 0°$	+	+
$180° > \tau_R > 90°$	+	-
$270° > \tau_R > 180°$	-	-
$360° > \tau_R > 270°$	-	+

and where $z_R = y_R = o$, τ_R is arbitrarily defined to be zero.

Similarly

$$\psi_R = \text{ARCTAN}\left(\frac{x_R}{\sqrt{y_R^2 + z_R^2}}\right) \quad 180° \geq \psi_R > -180° \qquad (48)$$

The quadrant assignments for ψ_R are somewhat simpler as the positive radical is always assumed:

Range of ψ_R	Sign of x_R
$90° > \psi_R > 0°$	+
$0° > \psi_R > -90°$	-

Since the missile will not ever fly substantially below the nominal surface of the Earth, no value of ψ_R need be defined for $x_R = y_R = z_R = o$.

The components of the velocity of the vehicle with respect to the local air mass depends, of course, on the winds. The wind is described by a constant speed and azimuth angle or by a table of speeds and a table of azimuth angles, each as a function of altitude. The wind is assumed to be horizontal and the air mass is assumed to move rigidly with the Earth, except for this wind. Therefore

$$\begin{bmatrix} V_{x_{LA}} \\ V_{y_{LA}} \\ V_{z_{LA}} \end{bmatrix} = \begin{bmatrix} V_{x_{LE}} + V_w \cos(A_w) \\ V_{y_{LE}} \\ V_{z_{LE}} + V_w \sin(A_w) \end{bmatrix} \qquad (49)$$

where A_w is the azimuth angle of the source of the wind, measured positively from the North toward East.

The components of this air velocity must be resolved in the rolling or nonrolling computational frame. Symbolically, this is

$$\begin{bmatrix} V_{x_{BA}} \\ V_{y_{BA}} \\ V_{z_{BA}} \end{bmatrix} = [\ell_B]^T [\ell_L]^T \begin{bmatrix} V_{x_{LA}} \\ V_{y_{LA}} \\ V_{z_{LA}} \end{bmatrix} \tag{50}$$

where subscript T denotes the transpose of a matrix. These rotation matrices are unitary, so that their transposes are their inverses.

The total velocity of the body with respect to the local air mass is

$$V_A = \sqrt{V_{x_{BA}}^2 + V_{y_{BA}}^2 + V_{z_{BA}}^2} \tag{51}$$

and the Mach number is given by

$$M = \frac{V_A}{c} \tag{52}$$

where the speed of sound, c, is calculated from the altitude by means of the standard atmosphere of Reference 3 or an atmosphere table supplied by the user.

The altitude of the vehicle is

$$h = \sqrt{x_R^2 + y_R^2 + z_R^2} - R_E \tag{53}$$

from the assumption of a spherical Earth, and the dynamic pressure is

$$Q = \frac{1}{2} \rho V_A^2$$

The atmospheric density is calculated by

$$\rho = \rho_A \ (D + 1)$$

where ρ_A is the atmospheric density from either the standard atmosphere or user supplied tables, and D is a density deviation table, versus altitude, supplied by the user.

INITIAL CONDITIONS

The user of a trajectory program wishes to give the initial conditions as measurements in an Earth-fixed frame of reference at the launch point, while the program computes in either inertial axes or body-fixed axes. Therefore X_R, Y_R, Z_R their derivatives, and $[\ell_B]$ must be expressed as functions of h, V_E, A_E, γ_E, ψ_E, τ_E, θ, $\bar{\alpha}$, ϕ, p, q, and r.

Since the Earth and inertial frames are initially coincident (Fig 6) the initial values of inertial latitude and longitude are equal to the Earth frame values input. Inverting Equations 47, 48, and 53 allows us to solve for the initial coordinates in terms of the altitude, radius of the Earth, latitude, and longitude.

The components of $\vec{V}_E$, the velocity of the vehicle with respect to the Earth, shown in Figure 4 resolved in the local frame, can be calculated by inverting Equations 56, 57, and 58 simultaneously:

$$A_E = \text{ARCTAN} \left[\frac{V_{z_{LE}}}{V_{x_{LE}}} \right] \qquad 360° > A_E \geq 0° \qquad (56)$$

where the quadrant assignments for A_E are again the traditional ones,

Range of A_E	Sign of $V_{z_{LE}}$	Sign of $V_{x_{LE}}$
$90° > A_E > 0°$	+	+
$180° > A_E > 90°$	+	-
$270° > A_E > 180°$	-	-
$360° > A_E > 270°$	-	+

and the special value of 0.0 is assigned to A_E when $V_{z_{LE}} = V_{z_{LE}} = 0.0$.

γ_E is

$$\gamma_E = \text{ARCTAN}\left[\frac{V_{y_{LE}}}{\sqrt{V_{x_{LE}}^2 + V_{z_{LE}}^2}}\right] \quad -90° \geq \gamma_E \geq 90° \qquad (57)$$

where γ_E has the sign of $V_{y_{LE}}$ and is zero when $V_{y_{LE}}$ is zero. V_E is

$$V_E = \sqrt{V_{x_{LE}}^2 + V_{y_{LE}}^2 + V_{z_{LE}}^2} \qquad (58)$$

Once we have obtained the components of $\vec{V}_E$ in the local frame, the components in the inertial frame can be calculated by inverting Equation 46.

The azimuth and elevation angles of the vehicle's velocity vector with respect to the local air mass are shown in Figure 4 and are computed from the local frame component of the vehicle's velocity with respect to the Earth, $V_{x_{LE}}$, $V_{y_{LE}}$, and $V_{z_{LE}}$. To obtain the velocity relative to the local air mass, we use Equation 49, solving for $V_{x_{LA}}$, $V_{y_{LA}}$, and $V_{z_{LA}}$, which can then be used for computing

$$A_A = \text{ARCTAN}\left[\frac{V_{z_{LA}}}{V_{x_{LA}}}\right] \quad 360° > A_A \geq 0° \qquad (59)$$

and

$$\gamma_A = \text{ARCTAN}\frac{V_{z_{LA}}}{\sqrt{V_{x_{LA}}^2 + V_{z_{LA}}^2}} \quad -90° \geq \gamma_A \geq +90° \qquad (60)$$

The sign and quadrant relations for A_A and γ_A are the same, respectively, as those of A_E and γ_E, defined for Equations 56 and 57.

The initial elements of the rotation matrix $[\ell_B]$ are also obtained in an inverted manner. The matrix $[\ell_B]$ is the transpose of the matrix product of a sequence of rotations transforming an axis system initially coincident with the inertial axes to be coincident with the rotating or non-rotating computational frame, which is initially coincident with the body-fixed frame. The sequence of rotations is

amount τ_R about the x_R axis, producing a frame x_R', y_R', z_R', (Fig 3)

amount $-\psi_R$ about the z_R' axis, producing a frame $x_{LE'}$, $y_{LE'}$, $z_{LE'}$ (Fig 3)

amount $-A_A$ about the y_{LE} axis, producing a frame $x_{LE'}'$, $y_{LE'}'$, $z_{LE'}'$ (Fig 4)

amount γ_A about the z_{LE}' axis, producing a frame $x_{LE'}''$, $y_{LE'}''$, $z_{LE'}''$, (Fig 4 & 5a)

amount θ-90° about the x_{LE}'' axis, producing a frame $x_{LE'}'''$, $y_{LE'}'''$ $z_{LE'}'''$ (Fig 5b)

amount $\bar{\alpha}$ about the y_{LE}''' axis, producing a frame x_A, y_A, z_A, (Fig 5b)

amount ϕ about the x_A axis, producing a frame $x_{BA'}$, $y_{BA'}$, $z_{BA'}$ (Fig 2)

A positive rotation about the X-axis of amount δ is represented by the rotation matrix

$$[\ell_x] = \begin{bmatrix} 1 & o & o \\ o & \cos(\delta) & \sin(\delta) \\ o & -\sin(\delta) & \cos(\delta) \end{bmatrix}$$

and, similarly, positive rotations about the Y-axis and Z-axis are represented by

$$[\ell_y] \quad \begin{bmatrix} \cos(\delta) & o & -\sin(\delta) \\ o & 1 & o \\ \sin(\delta) & o & \cos(\delta) \end{bmatrix}$$

and

$$[\ell_z] = \begin{bmatrix} \cos(\delta) & \sin(\delta) & o \\ -\sin(\delta) & \cos(\delta) & o \\ o & o & 1 \end{bmatrix}$$

Applying these representations to the sequence of rotations described above, we have for the initial value of the matrix transforming vectors from the inertial frame to the rotating or nonrotating computational frame

$$[\ell_B]^T = \begin{bmatrix} 1 & o & o \\ o & \cos(\phi) & \sin(\phi) \\ o & -\sin(\phi) & \cos(\phi) \end{bmatrix} \begin{bmatrix} \cos(\bar{\alpha}) & o & -\sin(\bar{\alpha}) \\ o & 1 & o \\ \sin(\bar{\alpha}) & o & \cos(\bar{\alpha}) \end{bmatrix}$$

$$\begin{bmatrix} 1 & o & o \\ o & \sin(\theta) & -\cos(\theta) \\ o & \cos(\theta) & \sin(\theta) \end{bmatrix} \begin{bmatrix} \cos(\gamma_A) & \sin(\gamma_A) & o \\ -\sin(\gamma_A) & \cos(\gamma_A) & o \\ o & o & 1 \end{bmatrix}$$

$$\begin{bmatrix} \cos(A_A) & o & \sin(A_A) \\ o & 1 & o \\ -\sin(A_A) & o & \cos(A_A) \end{bmatrix} \begin{bmatrix} \cos(\psi_R) & -\sin(\psi_R) & o \\ \sin(\psi_R) & \cos(\psi_R) & o \\ o & o & 1 \end{bmatrix}$$

$$\begin{bmatrix} 1 & o & o \\ o & \cos(\tau_R) & \sin(\tau_R) \\ o & -\sin(\tau_R) & \cos(\tau_R) \end{bmatrix} \qquad (61)$$

Given the matrix transformations $[\ell_B]$ and $[\ell_L]$, the components of velocity of the vehicle relative to the local air are calculated by Equation 50.

This then allows the computation of the angles of attack and sideslip illustrated in Figure 2.

$$\alpha = \text{ARCTAN } (V_{z_{BA}}/V_{x_{BA}})$$

and

$$\beta = \text{ARCTAN } (V_{y_{BA}}/V_{x_{BA}})$$

SPECIAL CALCULATIONS FOR OUTPUT

These calculations are made to either convert the state variables used for the integration procedure into variables convenient for a user at each printed interval or for special versions of the program. First we will consider the former.

The longitudinal and latitudinal ranges are the great circle arc length on the surface of the Earth from zero degrees longitude and latitude to the present position of the intersection of the radius vector of the projectile with the Earth's surface.

$$R_\tau \equiv R_E \tau_E \tag{62}$$

and

$$R_\psi \equiv R_E \psi_E \tag{63}$$

where

$$\tau_E = \text{ARCTAN } (Z_E/Y_E) \quad 360° \geq \tau_E \geq 0° \tag{64}$$

and

$$\psi_E = \text{ARCTAN } \left[\frac{X_E}{\sqrt{Y_E^2 + Z_E^2}} \right] \quad 180° \geq \psi_E > -180° \tag{65}$$

The sign conventions for the Earth's longitude and latitude are the same as those for Equations 47 and 48. The longitudinal range, is always positive and the latitudinal range, R_ψ, has the sign of ψ_E.

The Earth-fixed coordinates of position of the projectile are obtained from the inertial components of the position vector by

$$\begin{bmatrix} X_E \\ Y_E \\ Z_E \end{bmatrix} = [\ell_E] \begin{bmatrix} X_R \\ Y_R \\ Z_R \end{bmatrix} \tag{66}$$

The Earth and inertial frames are initially coincident and separate from each other by the spin of the Earth, which is about the Earth's X-axis (Fig 6). Therefore, the rotation matrix

$$[\ell_E] = \begin{bmatrix} 1 & o & o \\ o & \cos(\omega_E t) & \sin(\omega_E t) \\ o & -\sin(\omega_E t) & \cos(\omega_E t) \end{bmatrix} \tag{67}$$

is defined for any time of flight.

The time rate of change of the aerodynamic roll angle, ϕ, can be useful when the computational frame rolls with the body. A small oscillating value of $\dot{\phi}$, averaging zero, indicates that the projectile is in "lunar motion" or is "locked in," a condition which indicates yaw will grow. Therefore we compute $\dot{\phi}$ for printing.

$$\text{Tan}(\phi) = \frac{V_{y_{BA}}}{V_{z_{BA}}} \qquad \text{from Equation 44}$$

Taking a derivative with respect to time,

$$\dot{\phi} = \cos^2(\phi) \; \frac{V_{z_{BA}} \dot{V}_{y_{BA}} - V_{y_{BA}} \dot{V}_{z_{BA}}}{V_{z_{BA}}^2}$$

but

$$\cos(\phi) = \frac{V_{z_{BA}}}{\sqrt{V_{z_{BA}}^2 + V_{y_{BA}}^2}}$$

and

$$\dot{\vec{V}}_{BA} = \frac{d}{dt}\Big|_{BA} \vec{V}_{BA} = \frac{d}{dt}\Big|_{I} \vec{V}_{BA} - \vec{\omega} \times \vec{V}_{BA}$$

or

$$\frac{d}{dt}\Big|_{BA} \begin{bmatrix} V_{x_{BA}} \\ V_{y_{BA}} \\ V_{z_{BA}} \end{bmatrix} = \frac{d}{dt}\Big|_{I} \begin{bmatrix} V_{x_{BA}} \\ V_{y_{BA}} \\ V_{z_{BA}} \end{bmatrix} - \begin{bmatrix} p \\ q \\ r \end{bmatrix} \times \begin{bmatrix} V_{x_{BA}} \\ V_{y_{BA}} \\ V_{z_{BA}} \end{bmatrix}$$

where

$$\frac{d}{dt}\Big|_{I} \begin{bmatrix} V_{x_{BA}} \\ V_{y_{BA}} \\ V_{z_{BA}} \end{bmatrix} = \begin{bmatrix} F_x/m \\ F_y/m \\ F_z/m \end{bmatrix}$$

and

$$\begin{bmatrix} p \\ q \\ r \end{bmatrix} \times \begin{bmatrix} V_{x_{BA}} \\ V_{y_{BA}} \\ V_{z_{BA}} \end{bmatrix} = \begin{bmatrix} q V_{z_{BA}} - r V_{y_{BA}} \\ r V_{x_{BA}} - p V_{z_{BA}} \\ p V_{y_{BA}} - q V_{x_{BA}} \end{bmatrix}$$

therefore

$$\dot{\phi} = \frac{V_{z_{BA}} \left[\frac{F_x}{m} - r V_{x_{BA}} \right] - V_{y_{BA}} \left[\frac{F_z}{m} + q V_{x_{BA}} \right]}{V_{z_{BA}}^2 + V_{y_{BA}}^2} + p \tag{68}$$

Several of the alternate versions of the program require special calculations. PANOL 3 and PANOL 5 both allow the center of mass to lie off the centerline of the computational frame and allow the moment of inertia tensor to be non-diagonal. Both versions of the program are valid only after burnout, when the thrust and jet damping integrals are zero as is the gravity moment. (See Equation 7.) The gravity moment induced by the off-axis position of the center of mass is ignored as it averages to zero due to spin. For these conditions we can rewrite the rotational equation of motion in tensor-vector form, as

$$\left. \frac{d}{dt} \right|_I \vec{H} = \vec{\tau}_A + \vec{F}_A \times \vec{r}_c$$

where $\vec{H}$ is the angular momentum vector, $\vec{\tau}_A$ the aerodynamic torques, and $\vec{F}_A$ the aerodynamic forces; $\vec{r}_c$ is in this case the position of the center of mass with respect to the nominal burnout center of mass position (the computational frame origin).

If we fix the coordinate system to the projectile, the time rate-of-change operator in inertial space must be transformed:

$$\left. \frac{d}{dt} \right|_I = \left. \frac{d}{dt} \right|_{BA} + \vec{\Omega} \times$$

but the angular momentum becomes simply

$$\vec{H} = [I] \vec{\Omega}$$

where [I] is the moment of inertia tensor and is constant in body-fixed coordinates.

Therefore

$$[I] \left.\frac{d}{dt}\right|_{BA} \Omega = \vec{\tau}_A + \vec{F}_A \times \vec{r}_c + \vec{\Omega} \times \vec{H}$$

and

$$\left.\frac{d}{dt}\right|_{BA} \vec{\Omega} = [I]^{-1} \{\vec{\tau}_A + \vec{F}_A \times \vec{r}_c + \vec{\Omega} \times \vec{H}\} \qquad (69)$$

where

$$\vec{r}_c = \begin{bmatrix} o \\ y_c \\ z_c \end{bmatrix}$$

GUIDANCE AND CONTROL CALCULATIONS

The first requirement for a controlled vehicle is the definition of a target. Added to this program is a rectangular target in a vertical position. The target is of variable height and length. It is divided into a number of subrectangles, each of which has an intrinsic brightness defined by the user. The range, deflection, and orientation of the target can be input as tables versus time and are linearly interpolated for intermediate values of time.

Examining Figure 8, we see the target at longitude τ_T and latitude ψ_T on the surface of the Earth. It has a length (EL) and a height (HITE) and its unit normal ($\hat{n}$) is rotated by angle AZM from north toward west. In target coordinates, the center of a subrectangle (dA) is at y_{LOC}, z_{LOC}. In Earth coordinates, a vector from the origin to a given element

of the target (dA) is

$$\bar{R}_{dA} = \begin{bmatrix} (R_E + y_{LOC}) \sin(\psi_T) + z_{LOC} \sin(AZM)\cos(\psi_T) \\ (R_E + y_{LOC}) \cos(\psi_T)\cos(\tau_T) - Z_{LOC} \{\cos(AZM)\sin(\tau_T) + \\ \qquad \sin(AZM)\cos(\tau_T)\sin(\psi_T)\} \\ (R_E + y_{LOC}) \cos(\psi_T)\sin(\tau_T) + Z_{LOC} \{\cos(AZM)\cos(\tau_T) - \\ \qquad \sin(AZM)\sin(\tau_T)\sin(\psi_T)\} \end{bmatrix} \quad (70)$$

The position of the sensor in the missile coordinates is at x_s, y_s, z_s and since for controlled vehicles, the Earth is not allowed to rotate, the matrix $[\ell_B]$ transforms vectors from body frame effectively to Earth frame. Since R_E is the radius of the Earth and h the altitude of the vehicle, the sensor, in Earth-coordinates is at

$$R_s = \begin{bmatrix} (R_E + h) \sin(\psi_R) \\ (R_E + h) \cos(\psi_R)\cos(\tau_R) \\ (R_E + h) \cos(\psi_R)\sin(\tau_R) \end{bmatrix} + [\ell_B] \begin{bmatrix} x_s \\ y_s \\ z_s \end{bmatrix} \quad (71)$$

Therefore, the vector from a target element to the sensor is

$$\vec{R} = \vec{R}_s - \vec{R}_{dA}$$

A unit normal from any area element of the target is

$$\hat{n} = \begin{bmatrix} \cos(AZM)\cos(\psi_T) \\ \sin(AZM)\sin(\tau_T) - \cos(AZM)\cos(\tau_T)\sin(\psi_T) \\ -\sin(AZM)\cos(\tau_T) - \cos(AZM)\sin(\tau_T)\sin(\psi_T) \end{bmatrix} \quad (72)$$

The visible or projected area (of the differential area dA) in the direction of $\vec{R}$ is

$$A_p = \frac{\vec{R} \cdot \hat{n}}{|\vec{R}|} \tag{73}$$

which we multiply by the intrinsic brightness of the differential area and divide by the square of the distance between the differential area and the sensor.

The sensor is misaligned with the projectile X-axis by angle YAW in a plane rotated by angle ROL from the $x_B - y_B$ plane. A matrix $[\ell_s]$ produced by the rotation of amount ROL about the X_B-axis followed by a rotation of amount YAW about eh Z'_B axis describes this misalignment.

$$[\ell_s] = \begin{bmatrix} \cos(YAW) & \sin(YAW) & o \\ -\sin(YAW) & \cos(YAW) & o \\ o & o & 1 \end{bmatrix}$$

$$\begin{bmatrix} 1 & o & o \\ o & \cos(ROL) & \sin(ROL) \\ o & -\sin(ROL) & \cos(ROL) \end{bmatrix} =$$

$$\begin{bmatrix} \cos(YAW) & \sin(YAW)\cos(ROL) & \sin(YAW)\sin(ROL) \\ -\sin(YAW) & \cos(YAW)\cos(ROL) & \cos(YAW)\sin(ROL) \\ o & -\sin(ROL) & \cos(ROL) \end{bmatrix} \tag{74}$$

Therefore, $\vec{L}$ (a vector along the line of sight) is, in body frame,

$$\vec{L}\,[\ell_s]^{-1} \begin{bmatrix} 1 \\ o \\ o \end{bmatrix} = \begin{bmatrix} \cos(YAW) \\ \sin(YAW)\cos(ROL) \\ \sin(YAW)\sin(ROL) \end{bmatrix}$$

and in Earth frame,

$$\vec{L} = [\ell_B] \begin{bmatrix} \cos(YAW) \\ \sin(YAW)\cos(ROL) \\ \sin(YAW)\sin(ROL) \end{bmatrix}$$

Therefore, the angle between the line of sight of the seeker and the line from the seeker to the target area element is ALEPH.

$$ALEPH \equiv ARCCOS \left\{ -\frac{\vec{L} \cdot \vec{R}}{|\vec{R}|} \right\} \tag{75}$$

ALEPH may or may not be within the acceptance angle of the sensor (ACANG). If not, the element of target is ignored; if within the acceptance angle, the above-mentioned projected area (A_p) is multiplied by the intrinsic brightness and divided by the square of the distance to the area element to form a weighting factor (W_{ij}) and the vector $\vec{R}$ is resolved in sensor oriented components. If we examine Figure 9 we see a single plane (x-sensor, y-sensor) of the sensor-target relationship.

The y-sensor component of the image is a position y, which is proportional to the y_s component of the vector $\vec{R}$

$$y = K R_{y_s}$$

We wish to scale the image of the target such that when the i,j^{th} target element is at the limit of the acceptance angle its image element is at $y_{ij} = 1$.

$$TAN\ (ALEPH) = R^{ij}_{y_s} \Big/ R^{ij}_{x_s} = TAN\ (ACANG)$$

since

$$y^{ij} = 1 = K R^{ij}_{x_s} TAN\ (ACANG)$$

therefore

$$K = \frac{1}{R^{ij}_{x_s} TAN\ (ACANG)}$$

and

$$y^{i,j} = \frac{R^{i,j}_{y_s}}{R^{i,j}_{x_s} \text{ TAN (ACANG}}$$

The centroid is then approximated by

$$SUM = \sum_{ij} W_{ij}$$

and

$$YCNTR = \sum_{i,j} y^{ij} W_{ij} / SUM$$

A similar expression can be derived for the z - direction. The total strength of the signal to the sensor is SUM and the polar coordinates of the centroid of the image brightness can be calculated from the Cartesian coordinates in the usual way.

An empirical formula for the azimuthal and radial error in target centroid position due to vehicle roll rate interacting with a moving reticle is included.

The differential equations of motion of the gyroscope were developed by Dr. Gene Hopkins of Texas Instruments for the Tube Launched Guided Projectile. Much of the description of the gyro model is from Reference 4.

The gyro comprises a spherical gas-bearing torquers and a gimbal-angle readout system. Gyro motion is described with respect to a vehicle body-fized coordinate system by the angles θ_g (produced by a positive rotation about the vehicle y-axis and ψ_g (produced by a positive rotation about the [intermediate] z-axis). In matrix notation, the rotations take the form

$$[T_\theta] = \begin{bmatrix} \cos(\theta_g) & 0 & -\sin(\theta_g) \\ 0 & 1 & 0 \\ \sin(\theta_g) & 0 & \cos(\theta_g) \end{bmatrix}$$

and

$$[T_\psi] = \begin{bmatrix} \cos(\psi_g) & \sin(\psi_g) & o \\ -\sin(\Psi_g) & \cos(\psi_g) & o \\ o & o & 1 \end{bmatrix}$$

The total transformation is

$$[T_\psi]\,[T_\theta] = \begin{bmatrix} \cos(\psi_g)\cos(\theta_g) & \sin(\psi_g) & -\cos(\psi_g)\sin(\theta_g) \\ -\sin(\psi_g)\cos(\theta_g) & \cos(\psi_g) & \sin(\theta_g)\sin(\psi_g) \\ \sin(\theta_g) & o & \cos(\theta_g) \end{bmatrix} \quad (76)$$

This vehicle spin vector as expressed in body frame is

$$\vec{\omega} = p\,\hat{i} + q\,\hat{j} + r\,\hat{k}$$

and the total spin of the intermediate frame (x′, y′, z′) is

$$\vec{\omega}_1 = [T_\theta]\,\vec{\omega} + \dot{\theta}_g\,\hat{j}$$

The total spin of the gyro frame (that is, gyro spin less the axial component with respect to the body) with respect to inertial space is

$$\vec{\omega}_g = [T_\psi]\,\vec{\omega}_1 + \dot{\psi}_g\hat{k}_g$$

In gyro frame

$$\vec{\omega}_g = p_g\,\hat{i}_g = q_g\,\hat{j}_g + r_g\,\hat{k}_g$$

Solving for components, we get

$$p_g = p\cos(\psi_g)\cos(\theta_g) + (q + \dot{\theta}_g)\sin(\psi_g) - r\cos(\psi_g)\sin(\theta_g)$$

$$q_g = -p\sin(\psi_g)\cos(\theta_g) + (q + \dot{\theta}_g)\cos(\psi_g) + r\sin(\psi_g)\sin(\theta_g)$$

$$r_g = p\sin(\theta_g) + r\cos(\theta_g) + \dot{\psi}_g$$

Substituting the second equation into the first and eliminating $\dot{\theta}_g$ we get

$$p_g = [p \cos(\theta_g) - r \sin(\theta_g) + q_g \sin(\psi_g)] \sec(\psi_g)$$

From the second equation we can then find

$$\dot{\theta}_g = [q_g + p \sin(\psi_g) \cos(\theta_g) - r \sin(\psi_g) \sin(\theta_g)] \sec(\psi_g) - q$$

and from the third equation

$$\dot{\psi}_g = r_g - p \sin(\theta_g) - r \cos(\theta_g)$$

These show the exact kinematic description of the gyro gimbal motion. However, the angular momentum for a symmetric rotor is

$$\vec{H}_g = I_{x_r} (p_g + \omega_s) \hat{i}_g + I_{y_r} q_g \hat{j}_g + I_{y_r} r_g \hat{k}_g$$

where I_{x_r} is the axial moment of inertia and I_{y_r} the transverse moment of inertia of the rotor. We can write the equation of motion under the influence of applied torques, $\vec{M}$, as

$$\vec{M} = \frac{d\vec{H}}{dt}$$

and then by components

$$M_x = I_{x_r} (\dot{p}_g + \dot{\omega}_g) + q_g r_g (I_{y_r} - I_{x_r})$$

$$M_y = I_{y_r} \dot{q}_g + p_g r_g (I_{x_r} - I_{y_r}) - I_{x_r} \omega_s r_g$$

$$M_z = I_{y_r} \dot{r}_g + p_g q_g (I_{y_r} - I_{x_r}) - I_{x_r} \omega_s q_g$$

Since gyro rotor speed is considered constant, an expression for $\dot{\omega}_s$ is not needed. The moment of inertia ratio of the rotor is chosen such that the nutation frequency of the gyro is much above the spin frequency of the gyro. Therefore, the only mode of the gyro we need to analyze is the precession, for the other components will be outside the band width of the projectile and control system. These higher frequencies can be filtered out of the gyro pick-off signal. We need only a low frequency component of the resultant motion so we assume $\dot{q}_g = \dot{r}_g = o$ in the moment expressions and solve for q_g and r_g.

$$q_g = M_y \Big/ [p_g (I_{x_r} - I_{y_r}) + I_{x_r} \omega_s]$$

$$r_g = - M_z \Big/ [p_g (I_{x_r} - I_{y_r}) + I_{x_r} \omega_s]$$

Torque is applied to the rotor by coils on the outer frame of the gyro so the torque vector must be resolved into rotor coordinates:

$$\vec{\tau}_{App} = \tau_y \hat{j} + \tau_z \hat{k}$$

$$\vec{M} = [T_\psi] [T_\theta] \vec{\tau}_{App}$$

$M_x = o$ by the assumption of constant axial spin

$$M_y = \tau_y \cos(\psi_g) + \tau_z \sin(\psi_g) \sin(\theta_g) \qquad (77)$$

$$M_z = \tau_z \cos(\theta_g)$$

In summary, we have

$$p_g = [p \cos(\theta_g) - r \sin(\theta_g) + q_g \sin(\psi_g)] \sec(\psi_g)$$

$$q_g = -M_z \Big/ [p_g (I_{xr} - I_{y_r}) + I_{x_r} \omega_s]$$

$$r_g = M_y \Big/ [p_g (I_{x_r} - I_{y_r}) + I_{x_r} \omega_s] \tag{78}$$

$$\dot{\theta}_g = \{q_g + [p \cos(\theta_g) - r \sin(\theta_g)] \sin(\psi_g)\} \sec(\psi_g) - q$$

$$\dot{\psi}_g = r_g - p \sin(\theta_g) - r \cos(\theta_g)$$

for the exact low frequency response.

To simplify the equations and avoid numerical solution of the algebra, we examine several terms. In the equations for p_g and $\dot{\theta}_g$, since the gimbal angles are no more than a few degrees and the gyro is more nearly inertially still than the vehicle, $q_g \sin(\psi_g)$ is small compared with $r \sin(\theta_g)$ (on the average) and very small compared with $p \cos(\theta_g)$. The p_g equation can then be solved for $p \cos(\theta_g$ which can be substituted into the $\dot{\theta}_g$ equation, leaving

$$p_g \approx [p \cos(\theta_g) - r \sin(\theta_g)]/\cos(\psi_g)$$

$$\dot{\theta}_g \approx q_g \Big/ \cos(\psi_g) + p_g \sin(\psi_g)$$

Now the gyro gimbal angles can be integrated directly from initial conditions and body pitch, yaw, and spin rates. We begin with the p_g equation, then q_g and r_g, finally using the gyro rates for the $\dot{\theta}_g$ and $\dot{\psi}_g$ equations and integrating by numerical means. The interconnections of the gyro loop may be seen on Figure 7.

The output of the gyro loop in two dimensions is handed to the thruster logic which determines which of each opposed pair of lateral thrusters will be commanded on if the gas generator has been turned on and has not yet been exhausted. The valve diverting flow between the opposed thrusters is assumed to have a delay between the command to switch direction and the execution of the command. The flow actually switches completely and instantaneously.

A display in graphic form is provided at each time printout is generated. It displays a circle simulating the field of view of the sensor in body coordinates, an indication of the on or off status of each thruster, a mark indicating the centroid of the part of the target in view, the coordinates of the centroid, a statement as to whether control is on or off, and a statement as to whether the signal from the sensor is sufficiently strong to have the control system locked on.

REFERENCES

1. W. E. DeGrafft, "An IBM 7090 Six-Degree-of-Freedom Trajectory Program," NOLTR 64-225, Naval Ordnance Laboratory, White Oak, MD, February 1965

2. W. E. DeGrafft, "A Powered Flight Six-Degree-of-Freedom Trajectory Program for an IBM 7090 Computer," NOLTR 66-199, Naval Ordnance Laboratory, White Oak, MD, March 1967

3. S. L. Gerhard, "Users Manual for PANOL 6D Trajectory Programs," Information Report 496, Engineering Sciences Laboratory, Picatinny Arsenal, Dover, NJ, July 1970

4. Dr. Gene Hopkins, unpublished working paper, Texas Instruments Inc.

5. R.L. James, "A Three Dimensional Trajectory Simulation Using Six Degrees of Freedom with Arbitrary Wind," NASA TN-D-641, March 1961

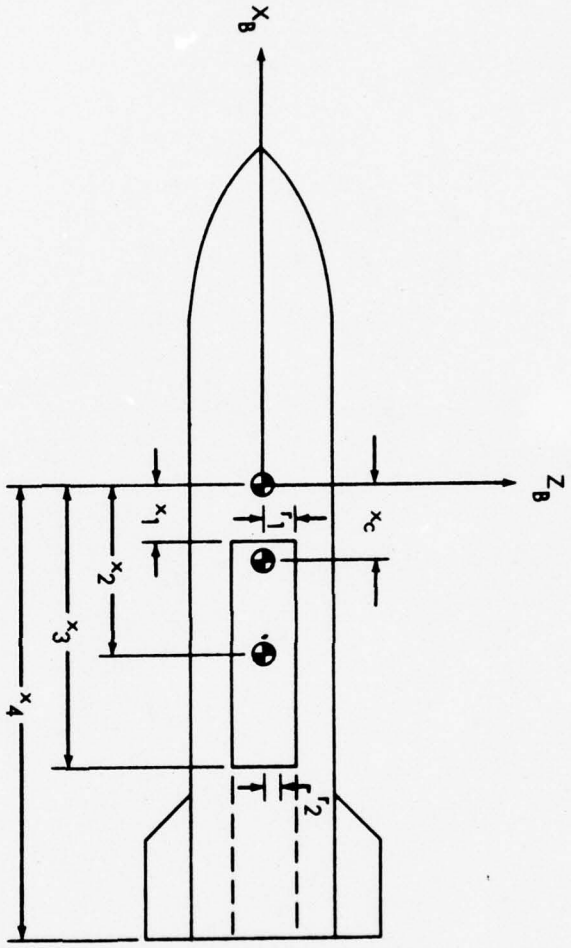

Fig 1 Rocket model

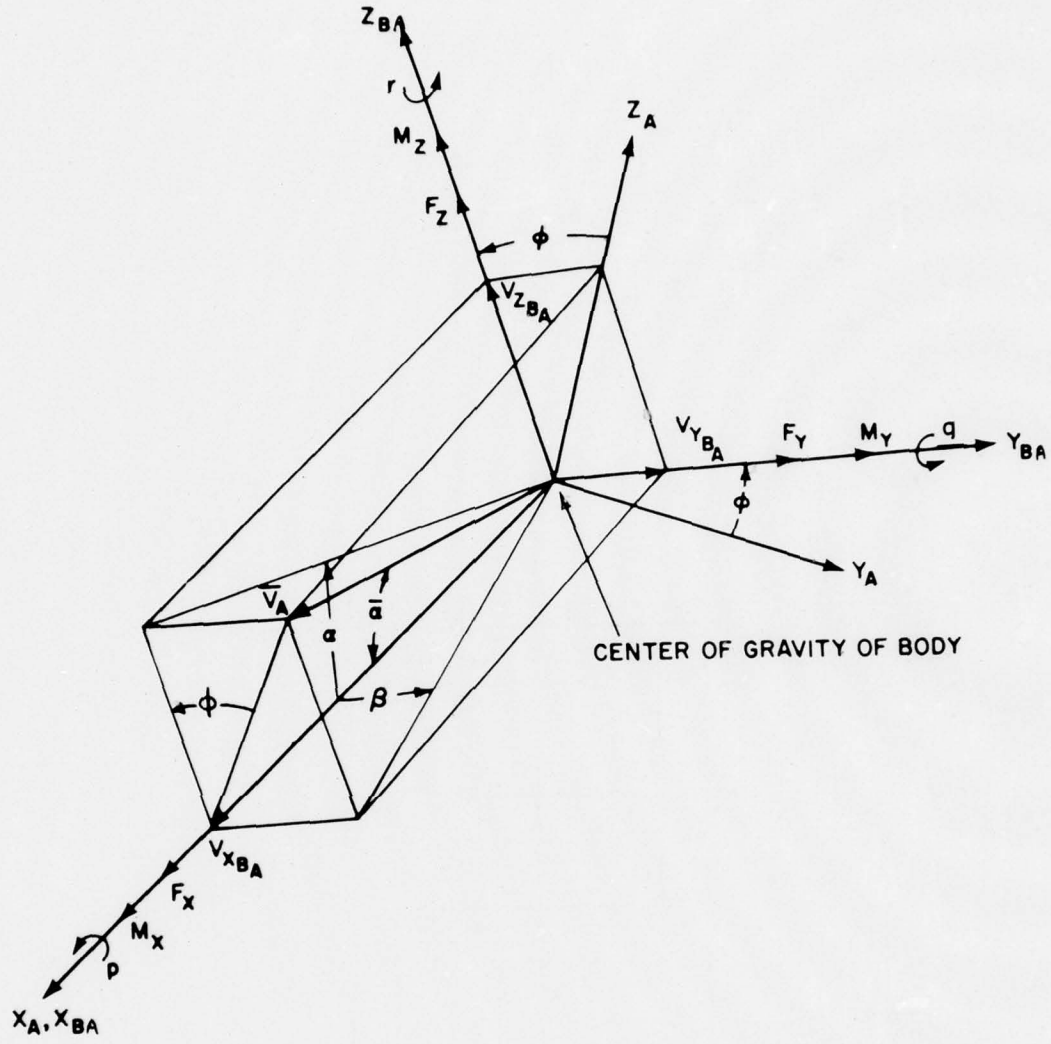

FIG. 2 AERODYNAMIC DATA AND BODY AXES SYSTEMS

Fig 2 Aerodynamic data and body axes systems

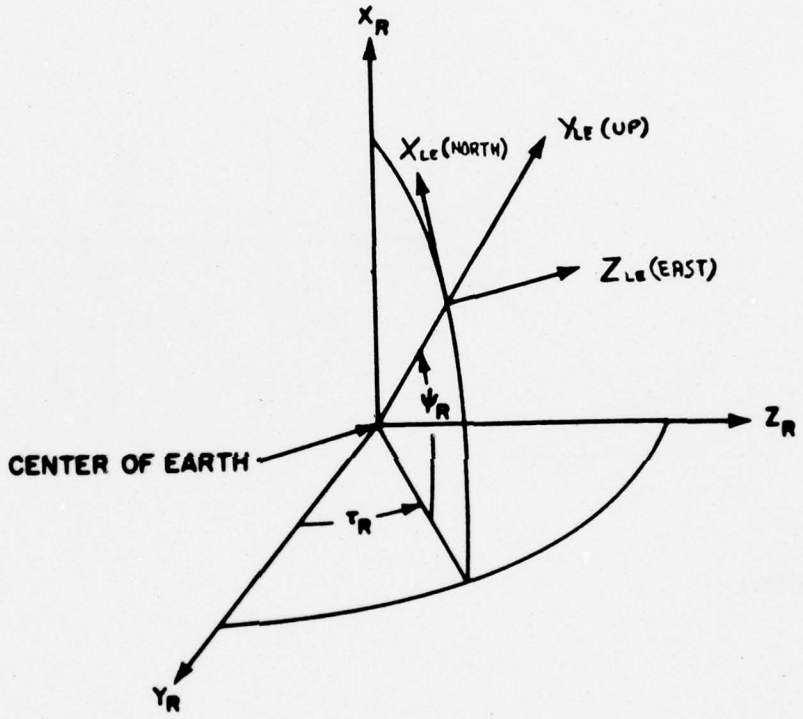

Fig 3 Inertial and local axes systems

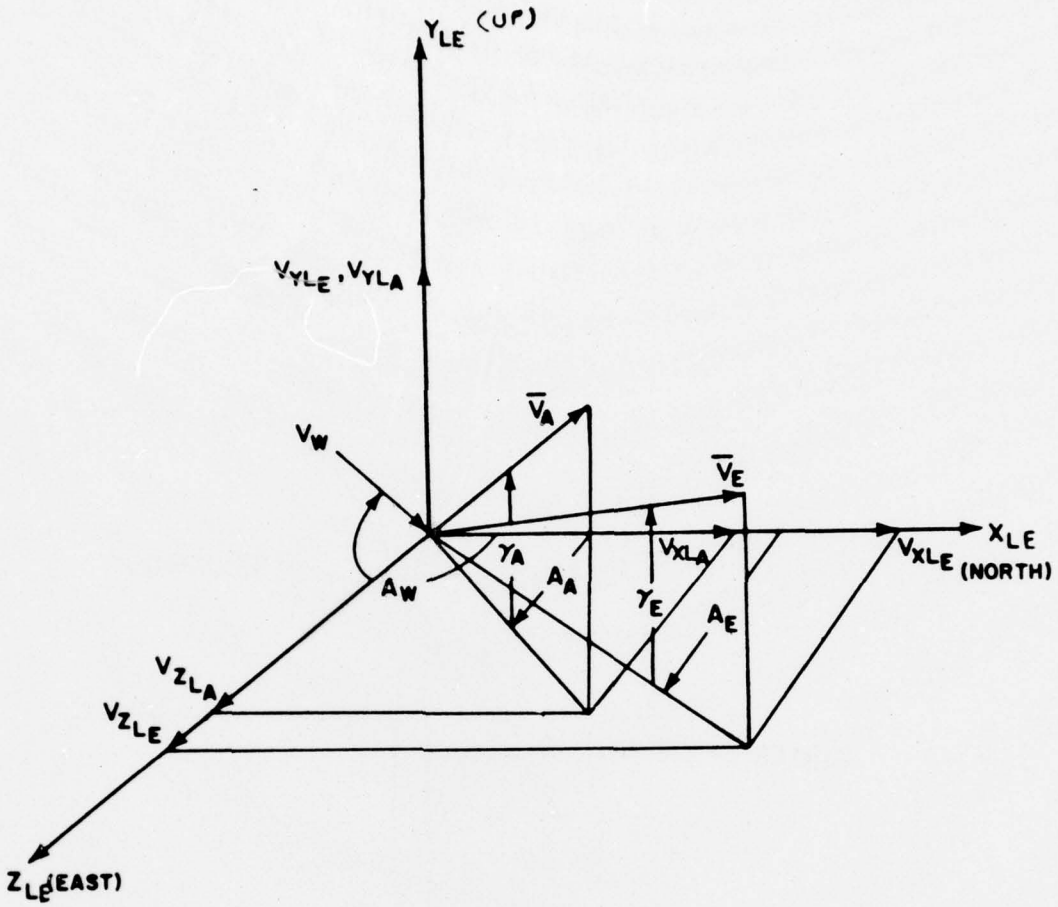

Fig 4 Velocity components in local axes system

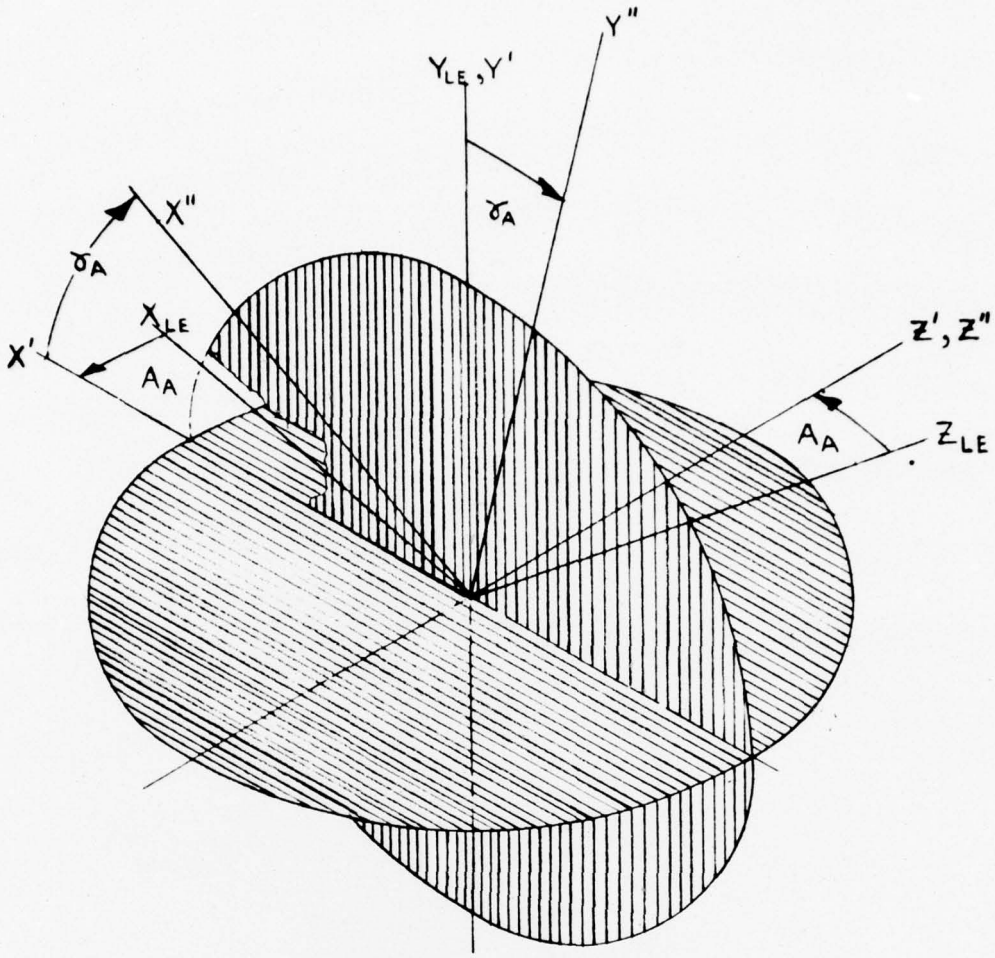

FIG.5A

Fig 5a Euler transformation from local axes to intermediate frame

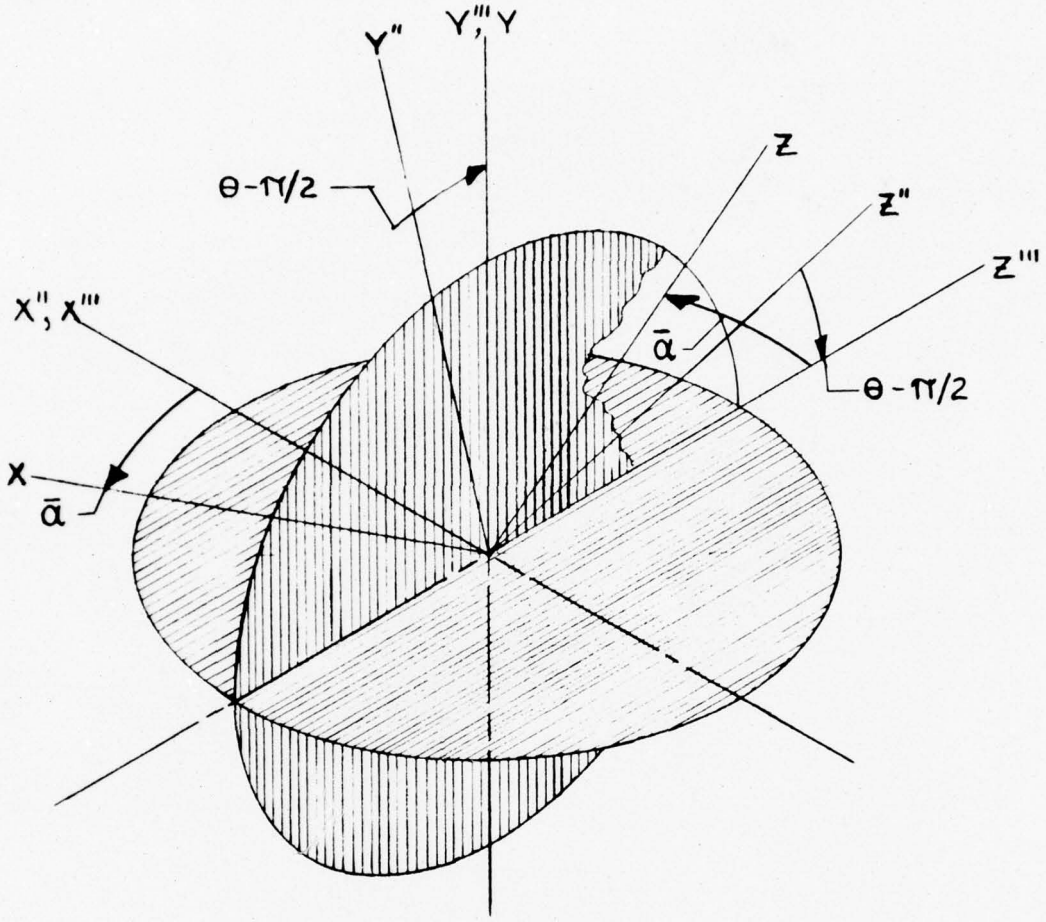

FIG.5B

5b Euler transformation from intermediate axes to computational frame

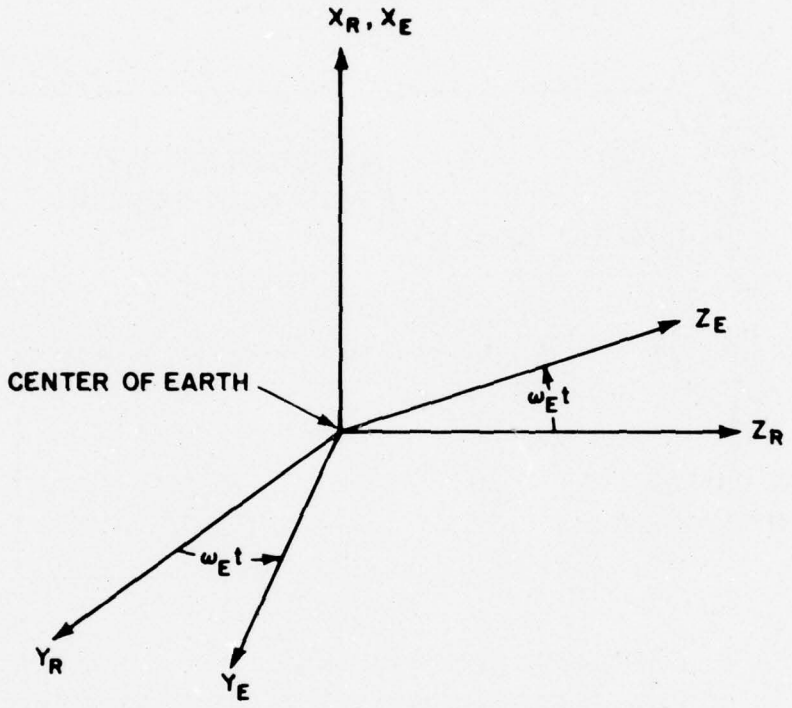

Fig 6 Earth and inertial axes systems

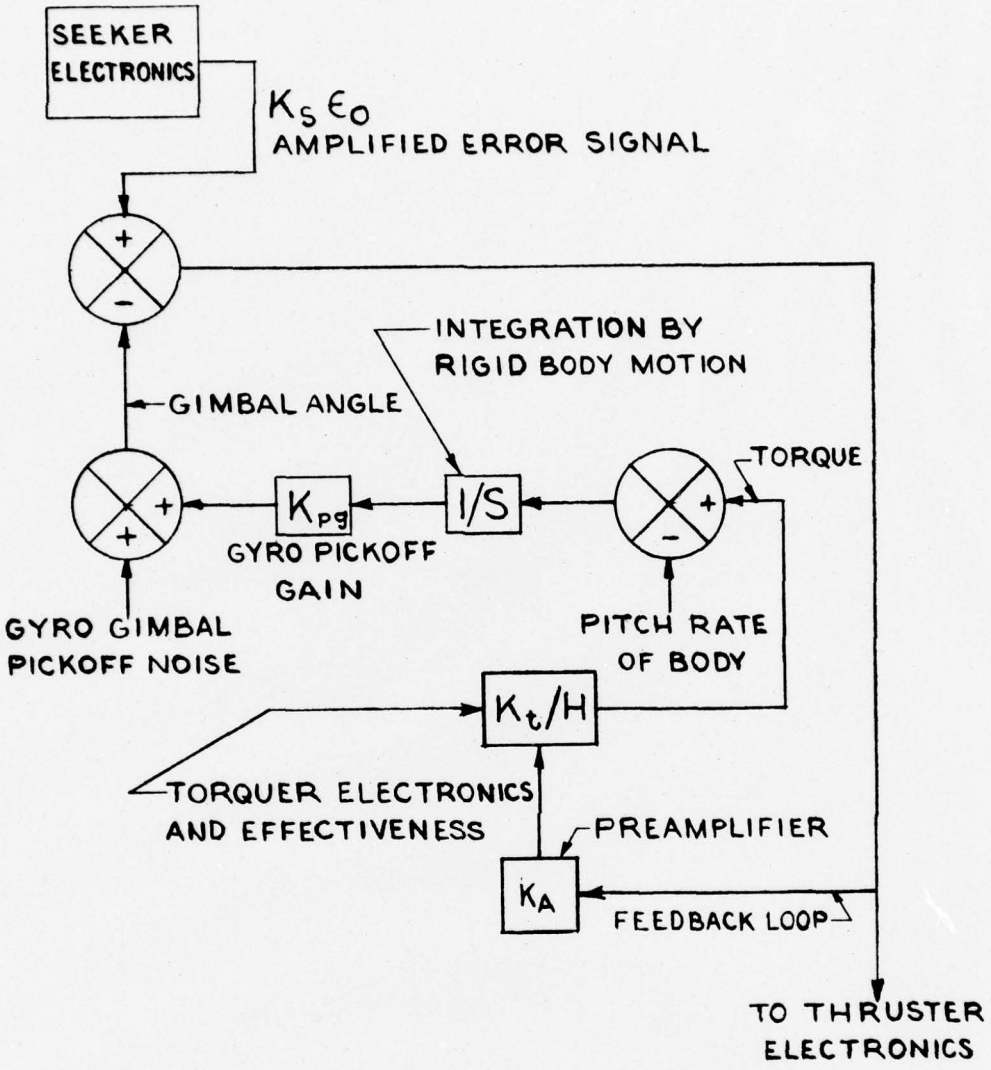

Fig 7 Guidance loop block diagram

Card No.	Col.	Fortran variable/symbol/description

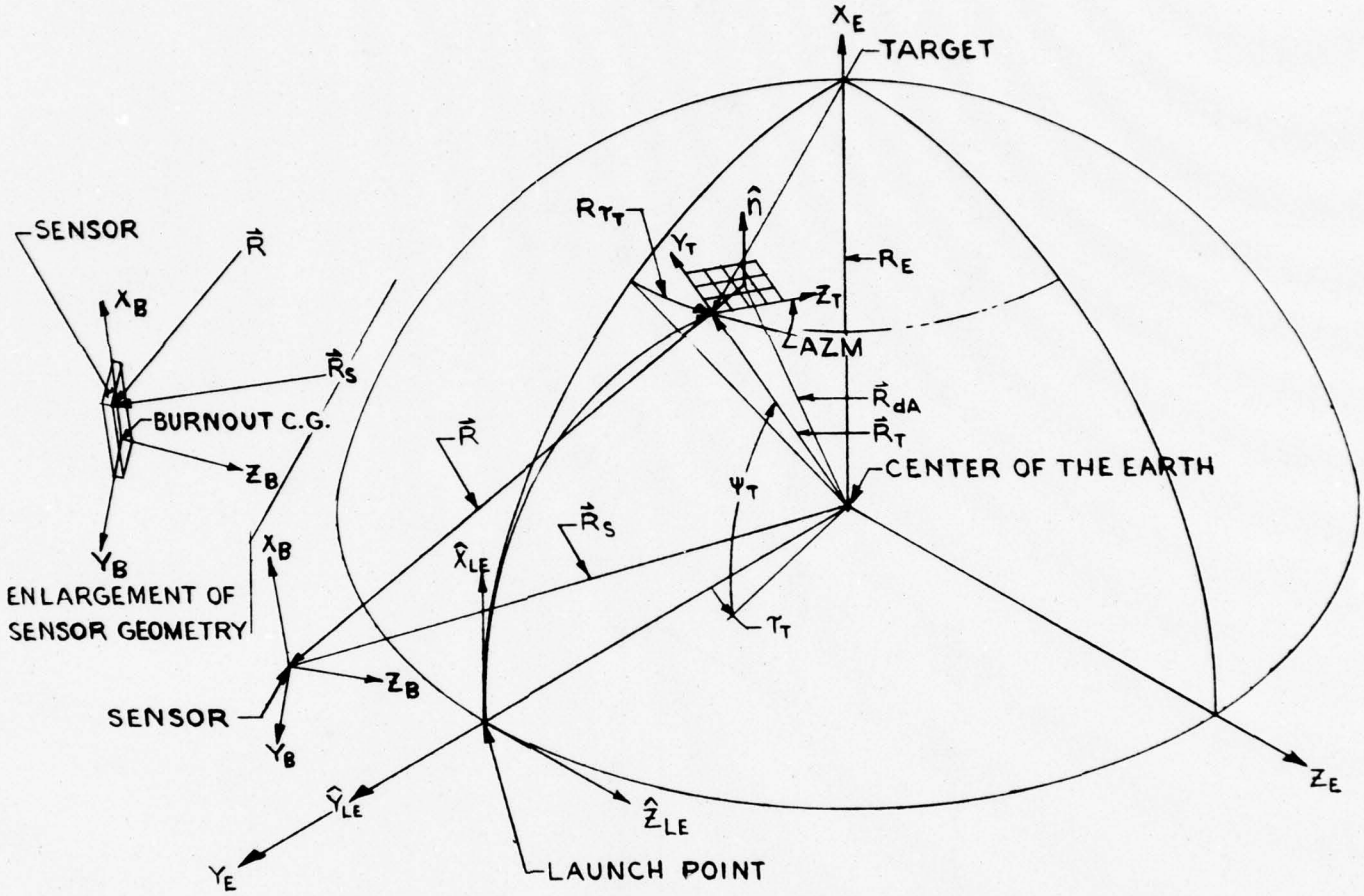

Fig 8 Target and sensor geometry

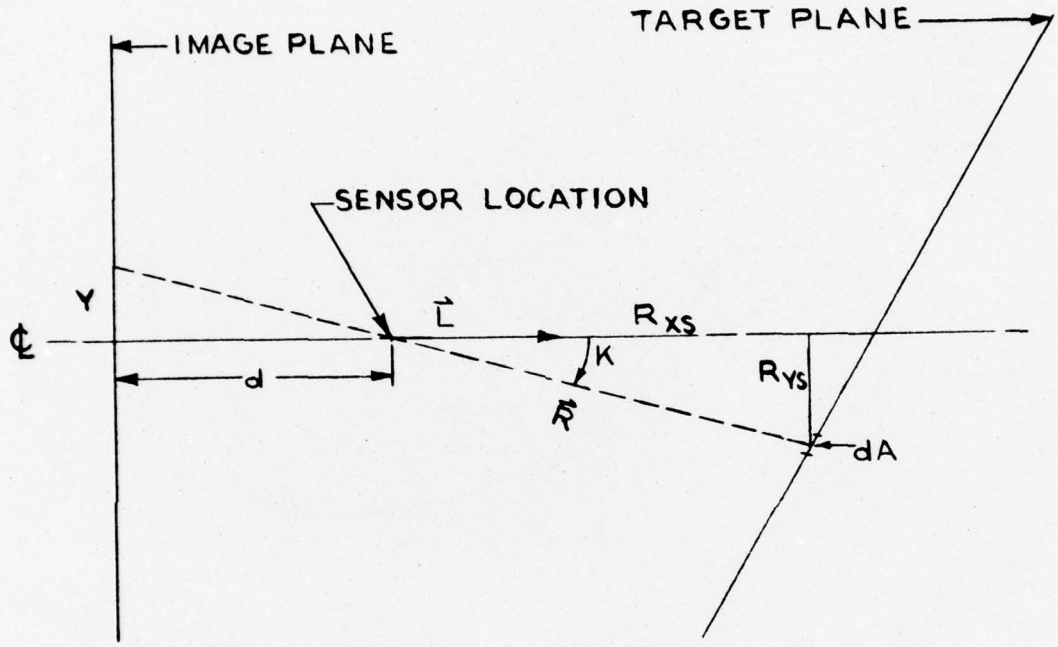

Fig 9 Sensor geometry

APPENDIX A

Computer Program Input Instructions

PROGRAM INPUT INSTRUCTIONS

Card No.	Col	Fortran variable/symbol/description
1	1-7	JO/ / Input 35 to omit wind tables input Input 37 to include wind tables
	8-14	NATMOS/ / Number of points in nonstandard atmosphere tables; max = 30
	15-21	NTHRST/ / Number of points in thrust table; max = 30
	22-28	KY (12)/ / Input 1 to omit printing of aerodynamic tables, otherwise input 0
	29-35	KY (13)/ / Input 1 to omit printing output formats 4 and 5
2	1-80	TYPE/ / Alphameric title for printing on output

Cards numbered 3 to 16 are aerodynamic coefficient tables and can be two dimensional or three dimensional. All tables are required for all versions of the program. An example of a two dimensional table is the axial force:

3-A	1-2	NCXM/ / Number of Mach numbers for C_X table; max = 16
	3-4	NCXA/ / Number of angles of attack (degrees) for C_X table; max = 10
3-B	1-72	TCXM/ / Table of Mach numbers for C_X table, E12 format, 6 per card, in ascending order
3-C	1-72	TCXA/ / Table of angles of attack for C_X table, E12 format, 6 per card, in ascending order
3-D-1	1-72	TCX/C_X/ Table of C_X coefficients, for lowest Mach number, one entry for each angle of attack, in order of ascending angle of attack, 6 per card, E12 format (may be more than one card)

Card No.	Col	Fortran variable/symbol/description
3-D-2 to 3-D-NCXM	1-72	TCX/C_X/ Table of C_X coefficients for second Mach number as card 3-D-1 above. Repeat until NCXM tables are supplied

An example of a three dimensional table is side force:

5-A	1-2	NCYM/ / Number of Mach numbers for C_y table; max = 6
	3-4	NCYA/ / Number of angles of attack for C_y table; max = 30
	5-6	NCYR/ / Number of roll angles for C_y table; max = 30
5-B	1-72	TCYM/ / Table of Mach numbers for C_y table
5-C	1-72	TCYA/ / Table of angles of attack (degrees) for C_y table
5-D	1-72	TCYR/ / Table of roll angles (degrees) for C_y table
5-E-1	1-72	TCY/C_y/ Table of C_y coefficients for lowest Mach number and angle of attack, one entry for each roll angle, in order of ascending roll angle, 6 per card, E12 format (may be more than one card)
5-E-2 to 5-E-NCYA	1-72	TCY/C_y/ Table of C_y for lowest Mach number and second lowest angle of attack as card 5-E-1 above. Repeat until NCYA tables are supplied; then repeat 5-E-1 to 5-E-NCYA for ascending values of Mach number until NCYM groups of tables are supplied

The following table gives the card numbers, coefficient names, dimension (dim) and maximum number of Mach numbers, angles of attack and roll angles allowed for each required table, in order.

Card No.	Coefficient name (symbol)	Dim	Max no. Mach	Max no. Alpha	Roll angle
3	Axial force (C_x)	2	16	10	
4	Spin induced axial force (C_{x_p})	2	6	5	
5	Induced side force (C_y)	3	6	10	30
6	Normal force (C_z)	3	16	10	15
7	Magnus force ($C_{y_{p_\alpha}}$)	2	16	10	
8	Trim force ($C_{z_{dA}}$)	2	6	5	
9	Induced roll moment (C_l)	3	6	10	30
10	Roll moment due to fin cant (C_{l_δ})	2	6	10	
11	Roll damping moment (C_{l_p})	2	16	10	
12	Pitching moment (C_m)	3	16	10	15
13	Induced side moment (C_m)	3	6	10	30
14	Pitch or yaw damping moment (C_{n_q})	2	16	10	
15	Magnus moment ($C_{m_{p_\alpha}}$)	2	16	10	
16	Trim moment ($C_{m_{\delta A}}$)	2	6	5	

Card No.	Col	Fortran variable/symbol/description
17	1-2	NHD/ / Number of points in atmospheric density deviation table; max = 30
	3-4	NHW/ / Number of points in wind velocity table; max = 30. Not needed for JO = 35 (card 1)
	5-6	NHA/ / Number of points in wind azimuth table; max = 30. Not needed for JO = 35 (card 1)
18	1-72	THD/ / Table of altitudes for atmospheric density deviation table, 6E12 format; max of 5 cards
19	1-72	TDN/ / Table of atmospheric density deviations, 6E12 format; max of 5 cards. Density = Density (1 + deviation)
20	1-72	THW/ / Table of altitudes for wind table (ft), 6E12 format; max of 5 cards
21	1-72	TWD/ / Table of wind velocities (ft/sec), 6E12 format; max of 5 cards
22	1-72	THA/ / Altitude table for wind azimuth (ft), 6E12 format; max of 5 cards
23	1-72	TA/ / Wind azimuth table (deg), 6E12 format; max of 5 cards
24	1-72	ALT/ / Table of altitudes for non-standard atmosphere (ft); omit if NATMOS = 0 on card #1; 6E12 format
25	1-72	TEMP/ / Table of temperatures for non-standard atmosphere (Rankine); 6E12 format
26	1-72	DENN/ / Table of densities for non-standard atmosphere ($lb\text{-}sec^2/ft^4$ or $slugs/ft^3$); 6E12 format
27	1-72	PRESS/ / Table of pressures for non-standard atmosphere (lb/ft^2); 6E12 format

Card No.	Col	Fortran variable/symbol/description
28	1-72	TIME/ / Table of times for thrust table (seconds), 6E12 format, omit if NTHRST = 0 on card #1; max of 5 cards
29	1-72	THRUST/ / Table of thrusts for above times, 6E12 format; same number of cards as TIME table
30	1-7	INTT/ / Input 1 for unpowered flight; input 2 for powered flight; 17 format
	8-14	NPUNCH/ / Input 1 to punch cards for FILM read program; omit for no cards desired
	15-21	NOGEES/ / Input 1 for no gravity, omit for standard gravity; I7 format
	22-28	KAUF/ / Input 0 for no tape output; input 1 for a tape of kinematic variables to start at launch; input 2 to start tape at apex; I7 format
	29-35	IGP/ / Input 1 to calculate geographic position on spherical Earth; omit for flat Earth approximation; if IGP = 0, Y (217) = Y (220) = Y (221) = 0
	36-42	KY (15)/ / Input a positive number for tables of target range and crossrange to be input on cards 42 & 43 in feet; input zero for a single value of each to be input on card 51 in feet; input a negative number if latitude and longitude are in radians
30	43-49	NUMPTS/ / Number of points in target position tables if KY (15) $\neq$ 0; maximum of 30
	50-56	NHT/ / Number of vertical subdivisions of the target for the brightness pattern

Card No.	Col	Fortran variable/symbol/description
	57-63	NLNTH/ / Number of horizontal subdivisions of the target for brightness pattern
	64-70	KY (16)/ / Plot frequency for seeker field of view and thruster logic state printed on logical unit 4; plots and every KY (16)th printed step
		10 I7 Format
31	1-7	KY (2)/ / Run number
	8-14	KY (3)/ / Mode of integration; Input 1 for Runge-Kutta, input 2 for Adams-Moulton; input 3 for Runge-Kutta with truncation error estimate; Adams-Moulton is recommended
	15-21	KY (4)/ / Number of differential equations for integration in principal loop; always input 19
	22-28	KY (5)/ / Always omit
	29-35	KY (6)/ / Always input 1
	36-42	KY (7)/ / Input 1 for including winds, omit for no winds
	43-49	KY (8)/ / Input 1 to periodically correct the numerically introduced non-orthogonality of the $[\ell_B]$ matrix; omit for no correction
	50-56	KY (9)/ / Print frequency for output; prints each KY (9) th integration step
	57-63	KY (10)/ / Print frequency of $[\ell_B]$ matrix to examine orthogonality

Card No.	Col	Fortran variable/symbol/description
	64-70	KY (11)/ / Aerodynamic symmetry options; Input 1 for 90° symmetry; Input 2 for 180° symmetry; Input 3 for 360° symmetry; input 4 for 60° symmetry; use 2 for a body of revolution
		All cards are 5E 14.6 FORMAT until further notice
32	1-14	Y (200)/h_t/ Terminal altitude, where calculations are to cease (feet)
	15-28	Y (201)/t_t/ Terminal time, when calculations are to cease (seconds)
	29-42	Y (202)/$\bar{\alpha}_t$/ Terminal total angle of attack, above which calculations cease (degrees)
	43-56	Y (203)/A_H/ Altitude above which atmosphere is assumed to have no effect (feet)
	57-70	Y (204)/ω_E/ Rotation speed of the Earth (radians/second); .00007292 is rotating, zero if not
33	1-14	Y (205)/Error/ Input 0. for integration interval to be adjusted to limit relative truncation error; input -1.0 to limit absolute truncation error
	15-28	Y (206)/ENE/ Input 0.0 to integrate with a fixed time step equal to Y (207); Input a positive value to adjust the integration step so that the interval lies between 10^{-ENE-3} and 10^{-ENE} seconds
	29-42	Y (207)/Δt_o/ Initial interval of integration (seconds)
	43-56	Y (208)/t_o/ Initial time (seconds)

Card No.	Col	Fortran variable/symbol/description
	57-70	Y (209)/K/ Input 0.0 for computational frame to be non-spinning; Input 1.0 for computational frame to spin with body
34	1-14	Y (215)/h/ Initial altitude (feet)
	15-28	Y (216)/V_E/ Initial speed with respect to the Earth (ft/sec)
	29-42	Y (217)/A_E/ Azimuth of launch velocity, measured from North toward East (degrees)
	43-56	Y (218)/γ_E/ Elevation angle of launch velocity (degrees)
	57-70	Y (219)/θ/ Determines the direction of the plane formed by the missile X-axis and the total wind vector if the initial angle of attack is not zero, see Figure 5 (degrees)
35	1-14	Y (220)/τ/ Initial longitude, if geographic position output desired (degrees); otherwise omit
	15-28	Y (221)/ψ/ Initial latitude, if geographic position output desired (degrees); otherwise omit
	29-42	Y (222)/$\bar{\alpha}$/ Initial total angle of attack (degrees)
	43-56	Y (223)/ϕ/ Initial roll angle of plane of angle of attack in computational frame (degrees)
	57-70	Y (224)/p/ Initial spin rate (radians/second)
36	1-14	Y (225)/q/ Initial pitch rate (radians/second)
	15-28	Y (226)/r/ Initial yaw rate (radians/second)
	29-42	Y (227)/V_w/ Wind speed (feet/second)

Card No.	Col	Fortran variable/symbol/description
	43-56	Y (228)/A_w/ Wind azimuth (degrees)
	57-70	Y (236)/δ/ Fin cant angle for spin acceleration coefficient (Same units as aerodynamic coefficient)
37	1-14	Y (230)/I_x/ Axial moment of inertia (slug-feet squared)
	15-28	Y (231)/I_y/ Transverse moment of inertia (slug-feet squared)
	29-42	Y (232)/I_z/ Transverse moment of inertia (slug-feet squared)
	43-56	Y (233)/m/ Mass of vehicle at burnout (slugs)
	57-70	Y (234)/A/ Vehicle reference area (square feet)
38	1-14	Y (235)/d/ Vehicle reference length (or diameter) (feet)
	15-28	Y (237)/δ_A/ Pitch aerodynamic asymmetry angle (Same units as $C_{m_{\delta A}}$)
	29-42	Y (238)/δ_B/ Yaw aerodynamic asymmetry angle (Same units as $C_{m_{\delta A}}$)
	43-56	Y (257)/x_{ec}/ Axial shift of burnout center of mass due to vehicle unbalance (inches)
	57-70	Y (258)/y_{ec}/ Laterial shift of burnout center of mass due to vehicle unbalance (inches)
39	1-14	Y (259)/λ/ Azimuthal orientation of lateral center of mass position due to vehicle unbalance (degrees)

Card No.	Col	Fortran variable/symbol/description
	15-28	Y (261)/H_1/ First Euler angle in transformation from computational frame to principal axis frame; rotation about the Z_{AB} axis (degrees)
	29-42	Y (262)/H_2/ Second Euler angle; about the Y′ axis (degrees)
	43-56	Y (263)/H_3/ Third Euler angle; about the X″ axis (degrees)
		Cards 40-44 are input for powered flight only; INTT on card 30 = 2
40	1-14	Y (210)/t_1/ Time when ignition occurs (seconds)
	15-28	Y (211)/t_2/ Time when burnout occurs (seconds)
	29-42	Y (212)/m_o/ Initial mass of vehicle (slugs)
	43-56	Y (213)/I_{x_o}/ Initial axial moment of inertia of vehicle (slug-ft^2)
	57-70	Y (214)/I_{y_o}/ Initial transverse moment of inertia of vehicle (slug-ft^2)
41	1-14	Y (240)/ε_1/ Thrust malalignment in yaw plane (radians)
	15-28	Y (241)/ε_2/ Thrust malalignment in pitch plane (radians)
	29-42	Y (242)/$\hat{X}_e$/ Axial location of nozzle exit in body for thrust malalignment (feet)
	43-56	Y (243)/$\hat{Y}_e$/ y-lateral location of nozzle for thrust malalignment (feet)
	57-70	Y (244)/$\hat{Z}_e$/ z-lateral location of nozzle for thrust malalignment (feet)

Card No.	Col	Fortran variable/symbol/description
42	1-14	Y (245)/$\dot{m}$/ Mass loss rate due to propellant burning, normally negative (slugs/sec)
	15-28	Y (246)/m_{p_o} / Initial mass of propellant (slugs)
	29-42	Y (247)/p_e/ Pressure of propellant gas at exit of nozzle (pounds/ft^2)
	43-56	Y (248)/A_e/ Nozzle exit area (feet squared)
	57-70	Y (249)/V_e/ Velocity of propellant gas at exit (feet/second)
43	1-14	Y (250)/X_{1_o} / Initial longitudinal position of front face of propellant grain with respect to origin of body frame (feet)
	15-28	Y (251)/X_{2_o} / Initial longitudinal position of center of mass of propellant grain (feet)
	29-42	Y (252)/X_{3_o} / Initial longitudinal position of rear face of propellant grain (feet)
	43-56	Y (253)/X_4/ Longitudinal position of nozzle exit plane for jet damping (feet)
	57-70	Y (254)/r_1/ Outer radius of propellant grain (ft)
44	1-14	Y (255)/r_{2_o} / Initial inner radius of propellant grain (feet)
	15-28	Y (256)/ρ_p/ Density of propellant grain (slugs/feet^3)
	29-42	Y (239)/X_{c_o} / Initial axial location of entire vehicle center of mass (feet)
	43-56	Y (260)/ / Specific impulse of propellant if mass loss rate is to be calculated (lb-sec/lb)

Cards 45 to 52 for PANOL 5 only

Use 6E12.0 Format Until Further Notice

Card No.	Col	Fortran variable/symbol/description
45	1-72	TARTIM/ / Table of times for target location, six per card, NUMPTS points total, see card 30; max of 5 cards (seconds)
46	1-72	TARAZM/ / Table of azimuth angles for the normal to the target surface out of the back side (degrees)
47	1-72	TARPSI/ψ_T/ Table of ranges to target versus time, feet, if KY (15) on card 30 is positive; table of latitude angles versus time, radians, if KY (15) is negative
48	1-72	TARTAU/τ_T/ Table of crossrange distance to target (feet), if KY (15) is positive; table of longitude angles versus time (radians) if KY (15) is negative
49		BRITAR/ / Table of brightness of the target sub-rectangles (energy output per square foot) from left to right, starting at the of the target and working upward in rows. It is suggested that a row at top and at bottom and a column at left and at right be held at zero brightness. The silhouette of the target can be traced inside this region and an estimate of the location of a hit can be made by the program
50	1-12	HTTAR/ / Height of the target (feet)
	13-24	ALNTAR/ / Length of the target (feet)
	25-36	YAWSNSR/ / Sensor malalignment with the vehicle X-axis (radians)

Card No.	Col	Fortran variable/symbol/description
	37-48	ROLSNSR/ / Roll angle of alignment plane of sensor (radians)
	49-60	ACANG/ / Half-apex-angle of the cone of the field of view of the sensor (degrees)
50	61-72	SIGMIN/ / Minimum received signal at the seeker for lockon - (energy per square foot); must contain allowances for size and efficiency of seeker as well as the chosen threshold
51	1-12	AZMTAR/ / Constant value for azimuth of target if no table input on card 46
	13-24	TAUTAR/ / Constant value for crossrange distance to target if no table input on card 48
	25-36	PSITAR/ / Constant value for range to target if no table input on card 47
	37-48	XSNSR/ / X position of sensor in body coordinates (feet)
	49-60	YSNSR/ / Y position of sensor in body coordinates (feet)
	61-72	ZSNSR/ / Z position of sensor in body coordinates (feet)
52	1-12	THRLVL/ / Thrust of a single steering jet when turned on (pounds)
	13-24	TIMON/ / Time steering jets turn on (seconds)
	25-36	TDEL/ / Time delay in steering jet valves; time from a command to switch thrust (eg, from left to right) until the command is carried out (seconds)

Card No.	Col	Fortran variable/symbol/description
	37-48	TIMOFF/ / Time steering jets shut off (seconds)
	49-60	XTHRUST/ / Longitudinal position of steering jets with respect to the center of mass, positive is toward the nose (feet)
		Cards 53 to 57 are for the TLGP version of PANOL 5 only
53	1-12	HGYRO/ / Time step for gyroscope integration (seconds)
	13-24	TGYRON/ / Time gyro turned on (seconds)
	25-36	TGYROFF/ / Time gyro turned off (seconds)
	37-48	GIX/I_{X_R} / Axial moment of inertia of gyro rotor (slug-ft^2)
	49-60	GIY/I_{Y_R} / Transverse moment of inertia of gyro rotor (slug-ft^2)
	61-72	GIZ/I_{Y_R} / Transverse moment of inertia of gyro rotor (slug-ft^2)
54	1-12	GYRMAS/M_R/ Mass of the gyro rotor (slugs)
	13-24	GYRX/ / X-position of gyro rotor in body frame (feet)
	25-36	GYRY/ / Y-position of gyro rotor in body frame (feet)
	37-48	GYRZ/ / Z-position of gyro rotor in body frame (feet)
	49-60	ALEPH/ / Initial pitch angle of gyro rotor (degrees)
	61-72	BET/ / Initial yaw angle of gyro rotor (degrees)

Card No.	Col	Fortran variable/symbol/description
55	1-12	GYRDX/ / Misalignment of rotor center of mass ahead of center of support (feet)
	13-24	GYRDY/ / Misalignment of rotor center of mass in Y-direction from center of support (ft)
	25-36	GYRDZ/ / Misalignment of rotor center of mass in Z-direction from center of support (ft)
	37-48	GYRWX/ / X-component of rotor initial spin rate (radians/second)
	49-60	GYRWY/ / Y-component of rotor initial spin rate (radians/second)
	61-72	GYRWZ/ / Z-component of rotor initial spin rate (radians/second)
56	1-12	FKA/K_A/ Feedback loop preamplifier gain in auto-pilot
	13-24	FKT/K_T/ Torque gain and effectiveness
	25-36	FKPG/K_{P_G} / Gyro attitude pickoff gain
	37-48	FKS/K_S/ Error signal amplifier gain
	49-60	AVGNGP/ / Mean of random noise in gyro pickoff
	61-72	SDNGP/ / Standard deviation of random noise in gyro pickoff
57	1-12	EPSGL/ε_{g_1}/ Maximum error signal (at which torques become nonlinear)
	13-24	EONE/e_1/ Maximum linear torque commanded out of torque rate gain
	25-36	ETWO/e_2/ Maximum torque commanded by torque rate gain

APPENDIX B

Output Format, Titles, and Units

FORMAT 1

TIME	H	VE	VA	MA
(seconds)	altitude (feet)	speed with respect to the Earth (feet/second)	speed with respect to the local air mass (feet/second)	Mach number (dimensionless)

QBAR	GAMMA E
dynamic pressure (pounds/ square ft)	elevation angle of velocity with respect to the Earth (degrees)

FORMAT 2

TIME	ALPHA BAR	PHI	PHI PRI	ALPHA
(seconds)	total angle of attack (degrees)	(degrees)	(degrees)	pitch angle (degrees)

BETA	Q	R
yaw angle (degrees)	pitch rate (radians/ second)	yaw rate (radians/ second)

FORMAT 3

TIME	DELT	P	RTAU	RPSI
(seconds)	time step (seconds)	spin rate (radians/ second)	deflection to the right or longitude (feet or degrees)	range or latitude (feet or degrees)
	PHIDC r			
	(radians/ second)			

FORMAT 4

TIME	FX	FY	FZ	MX
(seconds)	force in the X_{AB} direction (pounds)	force in the Y_{AB} direction (pounds)	force in the Z_{AB} direction (pounds)	torque in the X_{AB} direction (pound-ft)
	MY	MZ		
	torque in the Y_{AB} direction (pound-ft)	torque in the Z_{AB} direction (pound-ft)		

FORMAT 5

TIME	DDXR	DDYR	DDZR	DXR
(seconds)	acceleration in earth fixed X-direction (ft/second/ second)	acceleration in y-direction (ft/second/ second)	acceleration z-direction (ft/second/ second)	velocity in X-Earth direction (ft/second)

FORMAT 5 (Cont'd)

DYR	DZR
velocity in Y-Earth direction (ft/second)	velocity in Z-Earth direction (ft/second)

FORMAT 6

TIME	TH	WGT	XXI	YYI
(seconds)	thrust (pounds)	mass (slugs)	axial moment of inertia (slug-ft-squared)	transverse moment of inertia (slug-ft-squared)

ZZI	XC
transverse moment of inertia (slug-ft-squared)	center of mass (feet)

FORMAT 7

TIME	RANGE	DEFLECTION	HEIGHT
(seconds)	range or latitude (ft or degrees)	deflection or longitude (ft or degrees)	altitude (feet)

FX/M	FY/M	FZ/M
axial acceler-tion (ft/sec/sec)	normal acceleration (ft/sec/sec)	side acceleration (ft/sec/sec)

FORMAT 8

TIME	P	Q	R	PDOT
(seconds)	spin rate (radians/ sec)	pitch rate (radians/ sec)	yaw rate (radians/ sec)	spin acceler- ation (radians/ sec/sec)
	QDOT	RDOT	VXEB	
	pitch accelera- tion (radians/ sec/sec)	yaw accel- eration (radians/ sec/sec)	body X com- ponent of velocity with respect to the Earth (ft/second)	

FORMAT 9 (PANOL 5 only)

TIME	RNG TO TGT	SEEKR EPS Y	SEEKR EPS Z	THR 1
(seconds)	range to target (ft)	seeker error signal y com- ponent (degrees)	seeker error signal z com- ponent (degrees)	steering jet #1 thrust
	THR2	THR3	THR4	LOCKON
	steering jet #2 thrust	steering jet #3 thrust	steering jet #4 thrust	logical variable showing signal strength limit reached
	SIG STR	ALEPH	BET	
	signal strength received by sensor (energy/ second/ft^2)	gyro gymbol pitch angle (degrees)	gyro gymbol yaw angle (degrees)	

LIST OF SYMBOLS

A. Analytic Symbols

$\vec{a}$	Absolute acceleration of a mass particle within the geometric boundary of the vehicle
$\vec{a}_o$	Absolute acceleration of the origin of the body axes frame
$a_{o_x}, a_{o_y}, a_{o_z}$	Components of a_o in the body frame
$\vec{a}_r$	Acceleration of a mass particle within the geometric boundary of the vehicle measured with respect to the rolling body frame
A	Vehicle reference area
A_A	Azimuth of V_A in local frame
A_E	Azimuth of V_E in local frame
A_e	Rocket nozzle exit area
A_W	Azimuth of local wind
AZMTAR	Azimuth of $\hat{n}$, the unit normal from the back of the target
c	Speed of sound
C_X, C_Y, C_Z	Aerodynamic force coefficients defined in the body frame
C_L, C_M, C_N	Aerodynamic moment coefficients defined in the body frame
C_l, C_m, C_n	Aerodynamic moment coefficients defined in the aerodynamic data frame

C_{x_p}	$= \partial C_x / \partial (pd/2V_A)$
C_{y_p}	$= \partial C_y / \partial (pd/2V_A)$
$C_{z_{\delta A}}$	$= \partial C_z / \partial \delta A$
C_{ℓ_δ}	$= \partial C_\ell / \partial \delta$
C_{ℓ_p}	$= \partial C_\ell / \partial (pd/2V_A)$
C_{n_p}	$= \partial C_n / \partial (pd/2V_A)$
C_{m_q}	$= \partial C_m / \partial (qd/2V_A) = \partial C_m / \partial (rd/2V_A)$
$C_{m_{\delta A}}$	$= \partial C_m / \partial \delta A$
d	Vehicle reference diameter
D	Atmospheric density deviation function
$\vec{F}$	Resultant external force acting on the vehicle
F_x, F_y, F_z	Aerodynamic forces defined in the body frame
g_o	Acceleration due to gravity at earth's surface
h	Altitude of vehicle above earth's surface
[I]	Moment of inertia tensor (not necessarily diagonal)

I_x	Axial moment of inertia of vehicle at burnout
I_y	Transverse moment of inertia of vehicle about the Y_B axis at burnout
I_Z	Transverse moment of inertia of vehicle about the Z_B axis at burnout
$\vec{i}, \vec{j}, \vec{k}$	Unit vectors in body axes frame
$\hat{\ell}$	Unit vector in the direction of the line-of-sight of the sensor
$[\ell_B]$	Body to inertial frame transfer matrix
$[\ell_E]$	Inertial to earth frame transfer matrix
$[\ell_L]$	Inertial to local frame transfer matrix
$[\ell_S]$	Body to sensor frame transfer matrix
m	Mass of vehicle at burnout
m_p	Instantaneous propellant mass
m_g	Instantaneous mass of propellant gases within geometric boundary of vehicle
m_s	$m + m_p$
$\dot{m}$	Propellant mass flow rate, usually negative
M	Mach number
$\vec{M}$	Resultant external moment acting on the vehicle
M_x, M_y, M_z	Aerodynamic moments defined in the body frame

$\vec{n}_e$	Unit vector lying along inward normal to nozzle exit surface
P	Ambient atmospheric pressure
p, q, r	Components of angular velocity of vehicle in body frame
P_e	Static pressure of propellant gases at nozzle exit plane
Q	Dynamic pressure
$\vec{r}$	Position of a mass particle within geometric boundary of the vehicle with respect to the rolling, body-fixed frame
$\vec{r}_c$	Position of the instantaneous center of gravity of the vehicle with respect to the rolling, body-fixed frame
$\vec{r}_e$	Position of a point on the nozzle exit plane with respect to the rolling, body-fixed frame
r_1, r_2	Outer and inner radii of rocket motor propellant grain
$\hat{n}$	Unit normal from the target, out the back side
$\hat{R}$	Position of an arbitrary point within geometric boundary of vehicle with respect to the inertial frame
$\vec{R}$	Position of vehicle center of gravity with respect to the inertial frame
$\vec{R}_{dA}$	Position of a differential area in the target, in inertial frame
R_E	Radius of Earth
$\vec{R}_s$	Position of the sensor, in inertial frame

R_τ, R_ψ	Longitudinal and latitudinal range measured over the earth's surface
t	Time
t_1, t_2	Time of motor ignition and burnout
T	Thrust
$\vec{V}_A$	Velocity of vehicle with respect to local air mass
V_A	Speed of vehicle with respect to local air mass; equal to $\lvert \vec{V}_A \rvert$
$\vec{V}_E$	Velocity of vehicle with respect to Earth
V_E	Speed of vehicle with respect to earth; equal to $\lvert \vec{V}_A \rvert$
$\vec{V}_e$	Velocity of propellant gases at nozzle exit plane
V_e	Speed of propellant gases at nozzle exit plane; equal to $\lvert \vec{V}_e \rvert$
$\vec{V}_r$	Velocity of a mass particle within the geometric boundary of the vehicle with respect to the rolling body frame
V_{r_x}, V_{r_y}, V_{r_z}	Components of $\vec{V}_r$ in the rolling, body frame
V_W	Speed of local wind in the local frame
$V_{x_{BA}}$, $V_{y_{BA}}$, $V_{z_{BA}}$	Components of $\vec{V}_A$ in rolling or nonrolling, computational frame

$V_{x_{LA}}, V_{y_{LA}}, V_{z_{LA}}$	Components of $\vec{V}_A$ (velocity with respect to the local air mass) in local frame
$V_{x_{LE}}, V_{y_{LE}}, V_{z_{LE}}$	Components of $\vec{V}_E$ (velocity with respect to the Earth) in local frame
x_c	Longitudinal location of instantaneous center of gravity of entire vehicle with respect to body frame
x_e, y_e, z_e	Location of a point on the nozzle exit plane with respect to the rolling, body frame
$\hat{x}_e, \hat{y}_e, \hat{z}_e$	Location of centroid of nozzle exit area with respect to the rolling, body frame
x_o, y_o, z_o	Position of center of gravity of vehicle measured in the rolling body frame
x_1, x_3	Longitudinal position of front and rear faces of propellant grain with respect to origin of body frame
x_2	Longitudinal position of instantaneous center of gravity of propellant grain with respect to origin of body frame
x_4	Longitudinal position of nozzle exit plane with respect to the origin of the body frame
X_A, Y_A, Z_A	Aerodynamic data frame axes
X_B, Y_B, Z_B	Rolling or nonrolling, body frame axes
X_E, Y_E, Z_E	Earth frame axes
X_{LE}, Y_{LE}, Z_{LE}	Local frame axes

$X_{LOC}, Y_{LOC}, Z_{LOC}$	Target frame axes
X_R, Y_R, Z_R	Inertial frame axes, also position of vehicle center of gravity with respect to the inertial frame
α	Angle of attack
$\bar{\alpha}$	Total angle of attack
β	Angle of sideslip
γ_A	Elevation angle of $\vec{V}_A$ in local frame
γ_E	Elevation angle of $\vec{V}_E$ in local frame
δ	Average fin cant angle
$\delta A, \delta B$	Effective configurational asymmetry angle in pitch and yaw planes of rolling, body frame
$\varepsilon_1, \varepsilon_2$	Thrust misalignment angles in the yaw and pitch planes of rolling, body frame
θ	Orientation of plane of total angle of attack ($\bar{\alpha}$) and plane of elevation of $\vec{V}_A$ (γ_A)
ρ	Actual atmospheric density
ρ_A	Standard atmospheric density
ρ_e	Density of propellant gases at nozzle exit plane
ρ_g	Density of propellant gases within geometric boundary of vehicle
ρ_p	Density of propellant grain

τ_E	Earth longitude
τ_R	Inertial longitude
τ_T	Target longitude
φ	Azimuthal orientation of rolling, body-fixed frame with respect to $X_A - Z_A$ plane (angle of attack plane)
φ'	Azimuthal orientation of rolling body frame with respect to nonrolling body frame
ϕ	Azimuthal orientation of rolling or nonrolling computational frame with respect to $X_A - Z_A$ plane (angle of attack plane)
ϕ'	Dummy aerodynamic roll angle; reduced aerodynamic roll angle; φ modulo ξ, where ξ is the repeat roll angle of the aerodynamic symmetry
ψ_E	Earth latitude
ψ_R	Inertial latitude
ψ_T	Target latitude
$\vec{\omega}$	Angular velocity of a mass particle within the geometric boundary of the vehicle with respect to rolling body frame
ω_E	Rotational speed of earth
$\dot{(\ )}$	$\frac{d}{dt}$
$\ddot{(\ )}$	$\frac{d^2}{dt^2}$
$[\ ]^T$	Transpose of matrix

$[\ ]^{-1}$	Inverse of matrix
$(\ )_o$	Initial values unless otherwise specified
$(\ )_s$	Instantaneous value
$(\ )_t$	Value of a variable when calculations are automatically terminated

B. Fortran Array Designations and Definitions

KY (1)	Date
KY (2)	Run number
KY (3)	Mode of integration- 1 = Runge-Kutta 2 = Adams-Moulton 3 = Runge-Kutta with truncation error estimate
KY (4)	Number of differential equations; always input 19
KY (5)	Always zero
KY (6)	Always one
KY (7)	For no wind input zero; for wind input one
KY (8)	Zero = no $[\ell_B]$ correction; 1 = correct $[\ell_B]$
KY (9)	Print frequency for output
KY (10)	Print frequency for orthogonality of $[\ell_B]$
KY (11)	Rotational symmetry of body 1 = 90° symmetry 2 = 180° symmetry or body of revolution 3 = 360° symmetry 4 = 60° symmetry

AD-A044 539 ARMY ARMAMENT RESEARCH AND DEVELOPMENT COMMAND DOVER--ETC F/G 19/4
PANOL SIX DEGREES-OF-FREEDOM SYSTEM ANALYSIS AND USAGE.(U)
SEP 77 E M FRIEDMAN
ARLCD-TR-77025

UNCLASSIFIED

2 OF 2
AD
A044 539

END
DATE FILMED
10-77
DDC

KY (12)	Input one to omit printing of aerodynamic coefficient tables
KY (13)	Input one to omit printing output formats 4 and 5
KY (14)	Do not imput; used in MAIN to call SETUP in PANOL 3
KY (15)	Input a number greater than zero if the target position is input as tables in feet; input zero if a single value in feet; input a negative value if tables of latitude and longitude in radians
KY (16)	Plot frequency of seeker field of view
KY (17)-KY (20)	Not presently used

Y (1)-Y (9)	Rotation matrix, about X, by ϕ (Subroutine SETUP)
Y (10)-Y (18)	Rotation matrix, about Y, by $\bar{\alpha}$ (Subroutine SETUP)
Y (19)-Y (27)	Rotation matrix, about X, by θ-90° (Subroutine SETUP)
Y (28)-Y (36)	Rotation matrix, about Z, by γ_A (Subroutine SETUP)
Y (37)-Y (45)	Product of above matrices in subroutine SETUP; $[\ell_E]$ matrix in subroutine OUT
Y (46)	Cos (ψ_E) or cos (ψ_R) which are initially equal (Subroutine SETUP)
Y (47)	Sin (ψ_E) or sin (ψ_R) which are initially equal (Subroutine SETUP)
Y (48)	Cos (A_A) (Subroutine SETUP)
Y (49)	Sin (A_A) (Subroutine SETUP)
Y (52)	Cos (ψ_E) or cos (τ_R), which are initially equal (Subroutine SETUP)

Y (53)	$\sin(\tau_E)$ or $\sin(\tau_R)$, which are initially equal (Subroutine SETUP)
Y (54)	$\cos(\gamma_A)$ (Subroutine SETUP)
Y (55)	$\sin(\gamma_A)$ (Subroutine SETUP)
Y (56)	$\cos(\alpha)$ (Subroutine SETUP)
Y (57)	$\sin(\alpha)$ (Subroutine SETUP)
Y (58)	$\cos(\theta)$ (Subroutine SETUP)
Y (59)	$\sin(\theta)$ (Subroutine SETUP)
Y (66))	$V_{X_{LE}}$
Y (67)	$V_{Y_{LE}}$
Y (68)	$V_{Z_{LE}}$
Y (69)	X_E
Y (70)	Y_E
Y (71)	Z_E
Y (72)-Y (80)	$[\ell_L]$ array
Y (81. . .83)	Cross velocity in computational frame
Y (84. . .86)	Cross velocity in local frame
Y (87. . .89)	Sun vector in local frame (PANOL 4)
Y (90)	$V_{X_{BA}}$

Y (91)	$V_{y_{BA}}$
Y (92)	$V_{z_{BA}}$
Y (93)	V_A
Y (94)	R_τ
Y (95)	R_ψ
Y (96)-Y (104)	Intermediate storage
Y (105)	$C_{m_{\delta A}}$
Y (106)	Q, dynamic pressure
Y (107)-Y (109)	Intermediate storage
Y (110)	Mach number
Y (111)-Y (116)	Intermediate storage
Y (117)	C_{x_p}
Y (118)	C_{ℓ_δ}
Y (119)	C_{n_p}
Y (120)-Y (130)	Intermediate storage
Y (131)	ϕ'
Y (132)	C_x
Y (133)	C_y

Y (134)	C_z
Y (135)	C_ℓ
Y (136)	C_{ℓ_p}
Y (137)	C_m
Y (138)	C_n
Y (139)	C_{m_q}
Y (140)	C_{m_q} (originally yaw plane value; not now used)
Y (141)	$\dot{\phi}$
Y (142)	*Intermediate storage*
Y (143)	F_x; force in the x_{AB} direction (pounds)
Y (144)	F_y; total force in the y_{AB} direction (pounds)
Y (145)	F_z; *total force in the* z_{AB} *direction (pounds)*
Y (146)	M_x; total moment in the x_{AB} direction (pound-feet)
Y (147)	M_y; total moment in the y_{AB} direction (pound-feet)
Y (148)	M_z; total moment in the z_{AB} direction (pound-feet)
Y (149)-Y (162)	Intermediate storage
Y (163)-Y (189)	Used in Subroutine SETUP only
Y (190)-Y (199)	Intermediate storage
Y (200)	h_t; terminal altitude (feet)
Y (201)	t_t; terminal time (seconds)

Y (202)	$\bar{\alpha}_t$; terminal angle of attack (degrees)
Y (203)	A_H; altitude above which atmosphere is assumed negligible (feet)
Y (204)	ω_E; rotation rate of the Earth (radians/second)
Y (205)	Error; zero to limit relative truncation error, minus one to limit absolute truncation error
Y (206)	ENE; fixed step if zero, truncation error level if positive
Y (207)	Δt_o; initial integration step size (seconds)
Y (208)	t_o; initial time (seconds)
Y (209)	k; if zero, computational frame non-spinning if one, computational frame if body-fixed
Y (210)	t_1; time of main motor ignition (seconds)
Y (211)	t_2; time of main motor burnout (seconds)
Y (212)	m_o; initial mass of powered vehicle (slugs)
Y (213)	I_{x_o}; initial axial moment of inertia of powered vehicle (slug-ft^2)
Y (214)	I_{y_o}; initial transverse moment of inertia of powered vehicle (slug-ft^2)
Y (215)	h; initial altitude (feet)
Y (216)	V_E; initial speed with respect to the Earth (feet/sec)
Y (217)	A_E; azimuth of launch velocity (degrees)
Y (218)	γ_E; elevation angle of launch velocity (degrees)

Y (219)	θ; direction with respect to the Earth of plane of angle of attack, see Figure 5 (degrees)
Y (220)	τ; initial longitude if geographic output required (degrees)
Y (221)	ψ; initial latitude if geographic output required (degrees)
Y (222)	$\bar{\alpha}$; initial total angle of attack (degrees)
Y (223)	ϕ; initial direction of plane of angle of attack in computational frame (degrees)
Y (224)	p; initial spin rate (radians/second)
Y (225)	q; initial pitch rate (radians/second)
Y (226)	r; initial yaw rate (radians/second)
Y (227)	V_W; wind speed (feet/second)
Y (228)	A_W; wind direction azimuth (degrees)
Y (229)	R_E; radius of the Earth (feet)
Y (230)	I_x; axial moment of inertia (slug-feet-squared)
Y (231)	I_y; transverse moment of inertia (slug-feet-squared)
Y (232)	I_z; transverse moment of inertia (slug-feet-squared)
Y (233)	m; mass of vehicle at burnout (slugs)
Y (234)	A; vehicle reference area (square feet)
Y (235)	d; vehicle reference length (feet)
Y (236)	δ; effective configurational asymmetry angle (radians)
Y (237)	δ_A; pitch asymmetry angle (rad or deg depending on $C_{m_{\delta_A}}$)

Y (238)	δ_B; yaw asymmetry angle (rad or deg depending on $C_{m_{\delta_A}}$)
y (239)	x_{c_o}; initial axial location of entire vehicle center of mass (feet)
Y (240)	ε_1; thrust malalignment in yaw plane (radians)
Y (241)	ε_2; thrust malalignment in pitch plane (radians)
Y (242)	$\hat{x}_e$; axial location of nozzle exit in body for thrust malalignment (feet)
Y (243)	$\hat{y}_e$; y-lateral location of nozzle for thrust malalignment (feet)
Y (244)	$\hat{z}_e$; z-lateral location of nozzle for thrust malalignment (feet)
Y (245)	$\dot{m}$; mass loss rate from propellant burning (slugs/second)
Y (246)	m_{p_o}; initial mass of propellant (slugs)
Y (247)	p_e; pressure of propellant gas at exit of nozzle (pounds/ft^2)
Y (248)	A_e; nozzle exit area (square feet)
Y (249)	V_e; velocity of propellant gas at exit (feet/second)
Y (250)	x_{1_o}; initial position of front face of propellant grain (feet)
Y (251)	x_{2_o}; initial position of center of mass of propellant grain (feet)

Y (252)	x_{3_o} ; initial position of rear face of propellant grain (feet)
Y (253)	x_4; longitudinal position of nozzle exit plane for jet damping (feet)
Y (254)	r_1; outer radius of propellant grain (feet)
Y (255)	r_{2_o} ; initial inner radius of propellant grain (feet)
Y (256)	ρ_p; density of propellant grain (slugs/cubic feet)
Y (257)	x_{EC}; axial shift of burnout center of mass due to vehicle unbalance (inches)
Y (258)	y_{EC}; lateral shift of burnout center of mass due to vehicle unbalance (inches)
Y (259)	λ; azimuthal orientation of lateral center of mass position due to vehicle unbalance (degrees)
Y (260)	Specific impulse (lb sec/lb)
Y (261)	H_1; first Euler angle in transformation from computational frame to principal axis frame, about z_{AB} axis degrees)
Y (262)	H_2; second Euler angle, about y′ axis (degrees)
Y (263)	H_3; third Euler angle, about x″ axis (degrees)
Y (366)	Ma_x
Y (367)	Ma_y } Aerodynamic torques due to eccentric center of mass position
Y (368)	Ma_z

Y (369)	F_x/m	Accelerations in computational frame for output tape
Y (370)	F_y/m	
Y (371)	F_z/m	
Y (373)	V_x	Velocity components in computational frame for output tape
Y (373)	V_y	
Y (374)	V_z	
Y (375)-Y (383)		Available for use
Y (384)-Y (392)		Inertia tensor for principal axes
Y (393)-Y (401)		Intermediate storage
Y (402)-Y (410)		Inertia tensor for skewed axes
Y (Y (413)		Angular momentum $\vec{H}$
Y (416)		Omega time $\vec{H}$
Y (417)-Y (425)		Transpose of inertia tensor
Y (426)-Y (434)		Inverse of inertia tensor
Y (435)-Y (437)		Final sum of torques
Y (438)		Angle between sun vector and body axis (SIGMA)
Y (439)		THETA
Y (440)-Y (448)		Tensor RTEN to translate inertia tensor to off-axis center of mass
Y (449)-Y (451)		Missile axis components in Local Frame; Panol 4 only

Y (452)-Y (455)	q, r, $\dot{q}$, $\dot{r}$ in body-fixed (rotating frame
Y (456)	Spin number (non-dimensional spin)
Y (457)	Beta in non-spinning triad for plotting
Y (458)	Alpha in non-spinning triad for plotting
Y (460)-Y (468)	Inertia tensors in PANOL 3 only
Y (470)-Y (478)	
Y (480)-Y (488)	
Y (490)-Y (498)	
Y (601)-Y (3707)	Table storage for output

STATE VARIABLE-C ARRAY

C (1)	$\dot{X}_R$
C (2)	$\dot{Y}_R$
C (3)	$\dot{Z}_R$
C (4)	X_R
C (5)	Y_R
C (6)	Z_R
C (7)	p
C (8)	q
C (9)	r
C (10)	$[\ell_B]_{11}$
C (11)	$[\ell_B]_{21}$
C (12)	$[\ell_B]_{31}$
C (13)	$[\ell_B]_{12}$
C (14)	$[\ell_B]_{22}$
C (15)	$[\ell_B]_{32}$
C (16)	$[\ell_B]_{13}$

C (17)	$[\ell_B]_{23}$
C (18)	$[\ell_B]_{33}$
C (19)	φ'
C (20)-C (21)	Not presently used
C (22)	Error control
C (23)	Not presently used

STATE VARIABLE DERIVATIVE; D ARRAY

D (1)	$\ddot{X}_R$
D (2)	$\ddot{Y}_R$
D (3)	$\ddot{Z}_R$
D (4)	$\dot{X}_R$
D (5)	$\dot{Y}_R$
D (6)	$\dot{Z}_R$
D (7)	$\dot{p}$
D (8)	$\dot{q}$
D (9)	$\dot{r}$
D (10)	$[\dot{\ell}_B]_{11}$
D (11)	$[\dot{\ell}_B]_{21}$
D (12)	$[\dot{\ell}_B]_{31}$
D (13)	$[\dot{\ell}_B]_{12}$
D (14)	$[\dot{\ell}_B]_{22}$
D (15)	$[\dot{\ell}_B]_{32}$
D (16)	$[\dot{\ell}_B]_{13}$
D (17)	$[\dot{\ell}_B]_{23}$
D (18)	$[\dot{\ell}_B]_{33}$
D (19)	$\dot{\varphi}'$

DISTRIBUTION LIST

	Copy No.
Department of the Army Office, Chief of Research Development and Acquisition ATTN: DAMA-CB Washington, DC 20310	1
Department of the Army Office, Asst Chief of Staff for Force Development ATTN: CNNU Washington, DC 20310	2
Commander US Army Materiel Development and Readiness Command ATTN: DARCOM-SI-AT Research and Development Directorate 5001 Eisenhower Avenue Alexandria, VA 22304	3
Commander US Army Materiel Development and Readiness Command ATTN: DRCDL, Mr. N. Klein Research and Development Directorate 5001 Eisenhower Avenue Alexandria, VA 22333	4-5
Commander US Army Missile R&D Command ATTN: DRSMI-RDK, Mr. R. Deep Mr. R. E. Becht Redstone Arsenal, AL 35809	6 7
Redstone Scientific Information Center US Army Missile R&D Command ATTN: Chief, Document Section Redstone Arsenal, AL 35809	8

Commander/Director
Chemical Systems Laboratory
USA ARRADCOM
ATTN: Technical Library 9-10
Aberdeen Proving Ground, MD 21010

Project Manager
PM Cannon Artillery Weapons Systems
ATTN: DRCPM-CAWS-AM, Mr. F. Menke 11
Mr. M. Fisette 12
Mr. H. Noble 13
Mr. E. Zimpo 14
Dover, NJ 07801

PM for Selected Ammunition
ATTN: DRCPM-SA, Mr. B. Karin 15
Mr. M. Chase 16
Mr. L. Chaskes 17
Dover, NJ 07801

Director
Ballistic Research Laboratory
USA ARRADCOM
ATTN: DRDAR-BLL, Dr. C. Murphy 18
Mr. R. H. Krieger 19
Mr. L. MacAllister 20
Mr. R. McCoy 21
Mr. A. Platou 22
Aberdeen Proving Ground, MD 21005

Defense Documentation Center
Cameron Station
Alexandria, VA 22314 23-34

Commander
Harry Diamond Laboratories
ATTN: DRXDO-TI, Library 35-36
2800 Powdermill Road
Adelphi, MD 20783

Director
US Army Advanced Materiel Concepts Agency
2461 Eisenhower Avenue
Alexandria, VA 22314 37

Director
Advanced Research Projects Agency
Department of Defense
Washington, DC 20301 38

Chief, Bureau of Naval Weapons
Department of the Navy
ATTN: DIS-33 39
Washington, DC 20360

Commander
US Naval Surface Weapons Center
White Oak Laboratory
ATTN: Research Library 40
Mr. F. Regan 41
Mr. S. Hastings 42
Silver Spring, MD 20915

Commander
US Naval Surface Weapons Center
Dahlgren Laboratory
ATTN: *Technical Laboratory* 43
Dr. W. Chadwick 44
Mr. C. Wingo 45
Dr. T. Clare 46
Dahlgren, VA 22448

Commander & Director
Naval Ship Research and Development Center
ATTN: Aerodynamics Laboratory 47
Washington, DC 20007

Commander (Code 5557)
US Naval Weapons Center
ATTN: Technical Library 48
China Lake, CA 93555

Commander
Air Proving Ground Center (PGTRI)
ATTN: Technical Library 49
Mr. E. Sears 50
Mr. C. Butler 51
Eglin Air Force Base, FL 32542

Commander
US Army Combat Developments Command
Nuclear Agency
Fort Bliss, TX 79916 52

Assistant General Manager for
Military Applications
US Energy Research and Development Agency
Washington, DC 20545 53

Director
NASA Ames Research Center
ATTN: Mr. S. Treon 54
Moffett Field, CA 94035

Director
US Army Air Mobility R&D Laboratory
Moffett Field, CA 94035 55

Hq, US Air Force (AFRDDA)
Washington, DC 20330 56

Hq, Air Force Armament Laboratory (ATX)
Eglin Air Force Base, FL 32542 57

Hq, Air Force Systems Command (SCTS)
Andrews Air Force Base, MD 20331 58

Hq, Air Force Weapons Laboratory (WLX)
Kirtland Air Force Base, NM 87117 59

Commander
US Army Field Artillery School
ATTN: ATSF-CTD-L 60
Fort Sill, OK 73501

General Electric Company
Armament Department
ATTN: Mr. R. H. Whyte 61
Room 1412
Lakeside Avenue
Burlington, VT 05401

Sandia Laboratories
ATTN: Aerodynamics Department 62
Mr. H. Vaughn 63
Mr. A. Hodapp 64
Mr. W. Curry 65
PO Box 5800
Albuquerque, NM 87115

Director
USAMSAA
ATTN: Mr. C. T. Odom 66
Mr. N. DiGiacomo 67
Aberdeen Proving Ground, MD 21005

Defense Research Establishment Valcartier
ATTN: Mr. B. Cheers 68
PO Box 880
Courcelette, PQ, Canada GOA IRO

Royal Armament Research and Development
Establishment
ATTN: Dr. R. Fancett, GR2 Branch 69
Mr. W. Clayden, GR3 Branch 70
Fort Halstead, Sevenoaks
Kent, England

Weapons Research Establishment
ATTN: Mr. K. C. Thompson, Aerospace Division 71
GPO Box 2151
Adelaide, SA 5001 Australia

Commander
US Army Armament Research and
Development Command
ATTN: DRDAR-TSS 72-76
DRDAR-LC, Dr. J. Frasier 77
DRDAR-LCA, Dr. E.G. Sharkoff 78-79
DRDAR-LCU, Mr. A. Moss 80
DRDAR-LCU-T, Mr. G. Jackman 81
DRDAR-LCA-F, Mr. A.A. Loeb 82-84
Mr. D.H. Mertz 85-87
Mr. R.W. Kline 88
Mr. T.D. Hoffman 89
Mr. S. D. Kahn 90
Mr. C.H. Ng 91
Mr. E. Brown 92
Mr. E. Falkowski 93
Mr. H. Hudgins 94
Mr. W. O'Keefe 95
Mr. S. Wasserman 96
Mr. E. Friedman 97-101
Mr. G. Fleming 102
DRDAR-LCU-D, Mr. D. Costa 103
DRDAR-LCN-DP, Mr. C. Spinelli 104
DRDAR-LCU-T, Mr. R. Corn 105
Mr. F. Diorio 106
DRDAR-LCU-DP, Mr. M. Margolin 107
DRDAR-MS-MSM, Mr. B. Barnett 108
Mr. E. Lacher 109
DRDAR-LCN-F, Dr. L. Nichols 110-114
Mr. F. Scerbo 115-116
Dover, NJ 07801